Neuron

Article

Selective loss of *Scn2a* in ventral tegmental area dopaminergic neurons leads to dopamine system hypofunction and autistic-like behaviors

Graphical abstract

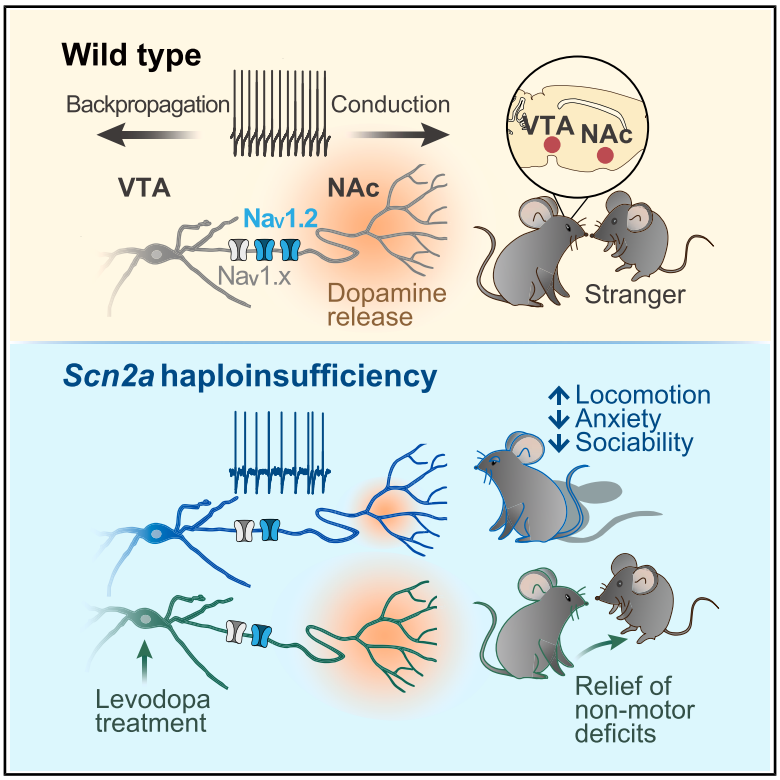

Highlights

- *Scn2a* is the predominant Na^+ channel isoform in dopaminergic neurons (DANs)
- Deletion of *Scn2a* in DANs reduces neuronal excitability and dopamine release
- *Scn2a* loss in VTA DANs alone recaptures autistic-like behaviors of *Scn2a*$^{+/-}$ mice
- Levodopa treatment alleviates non-motor behavior deficits in *Scn2a*$^{+/-}$ mice

Authors

Liang Li, Qi Huang, Jiahao Hu, ..., Jie He, Bo Li, Yousheng Shu

Correspondence

yousheng@fudan.edu.cn

In brief

SCN2A loss-of-function mutations are a high-risk factor for autism. Li et al. show that selective *Scn2a* deficiency in VTA dopaminergic neurons or global haploinsufficiency in *Scn2a*$^{+/-}$ mice causes dopamine system hypofunction. Levodopa treatment at an appropriate dosage can alleviate non-motor autistic-like behaviors, including insufficient anxiety and social deficits.

Li et al., 2025, Neuron *113*, 1–18
September 17, 2025
https://doi.org/10.1016/j.neuron.2025.06.003

CellPress

Neuron

CellPress

Article

Selective loss of *Scn2a* in ventral tegmental area dopaminergic neurons leads to dopamine system hypofunction and autistic-like behaviors

Liang Li,[1,2,5] Qi Huang,[1,2,5] Jiahao Hu,[1,2] Mengmeng Jin,[3] Yizhou Zhuo,[4] Wei Ke,[1,2] Quansheng He,[1,2] Yujie Xiao,[1,2] Xiaoxue Zhang,[1] Weisheng Wang,[1] Tian-lin Cheng,[1] Yilin Tai,[1] Feifan Guo,[1] Jintai Yu,[2] Yulong Li,[4] Jie He,[3] Bo Li,[1,2] and Yousheng Shu[1,2,6,*]

[1]Department of Neurology, Jinshan Hospital, Institute for Translational Brain Research, State Key Laboratory of Brain Function and Disorders, MOE Frontiers Center for Brain Science, MOE Innovative Center for New Drug Development of Immune Inflammatory Diseases, Fudan University, Shanghai 201508, China

[2]Department of Neurology, Huashan Hospital, Fudan University, Shanghai 200032, China

[3]Center for Excellence in Brain Science and Technology, Chinese Academy of Sciences, Shanghai 200031, China

[4]State Key Laboratory of Membrane Biology, Peking University School of Life Sciences, Beijing 100871, China

[5]These authors contributed equally

[6]Lead contact

*Correspondence: yousheng@fudan.edu.cn

https://doi.org/10.1016/j.neuron.2025.06.003

SUMMARY

Dopamine hypothesis has been proposed as a mechanism of autism spectrum disorder (ASD), a neurodevelopmental disorder closely associated with genetic mutations. Loss-of-function mutation of *SCN2A*, which encodes the voltage-gated Na^+ channel $Na_V1.2$, is a high risk factor for autism, but whether its pathogenesis is attributable to dopamine system dysfunction remains unclear. Here, we found that *Scn2a* is the predominant isoform and contributes largely to Na^+ currents along the somato-axonal axis of dopaminergic neurons (DANs) in mouse ventral tegmental area (VTA). Complete deletion of *Scn2a* in VTA DANs reduces their spiking activity and dopamine release, leading to hyperactivity, impaired sociability, and insufficient anxiety. Similar alterations were observed in *Scn2a* heterozygous mice. Importantly, acute treatment with levodopa alleviates non-motor behavior deficits. Together, the results reveal that *Scn2a* loss in VTA DANs alone causes autistic-like behaviors through a dopamine-hypofunction mechanism and also provide a possible pharmacotherapy through dopamine replacement for ASD with *SCN2A* mutations.

INTRODUCTION

Autism spectrum disorder (ASD) is an aberrant neurodevelopmental condition characterized by impairments in sociability and restricted/repetitive behaviors.[1,2] There is currently no available pharmacological treatment proven effective for the core symptoms, largely due to the lack of clear molecular, cellular, and circuit mechanisms of pathogenesis. Malfunction of the dopamine system has been observed in individuals with ASD, such as lower activity of dopamine synthesis and aberrant connectivity of the mesolimbic reward pathway.[3–5] In ASD mouse models, altered synaptic inputs on dopaminergic neurons (DANs) in the ventral tegmental area (VTA) could cause social deficits.[6–8] Previous studies through genetic manipulation also reported a causal link of the spiking activity of VTA DANs to sociability, including social interactions and social novelty preference.[7,9,10] However, whether pathological alterations of VTA DAN activity directly cause autistic-like behaviors remains unclear.

Previous studies revealed a strong association of ASD with *de novo* gene mutations, most of which are closely linked to the modulation or formation of synapses.[11–15] Another important class of genes are those regulating neuronal signal generation and excitability, including *SCN2A*, which encodes the α-subunit of voltage-gated Na^+ channel (Na_V) 1.2, an isoform critical for action potential (AP) generation and propagation in many types of neurons.[16–23] *SCN2A* loss-of-function mutations are a high risk factor for ASD and intellectual disability.[24,25] Loss of *Scn2a* in mice, however, shows a cell-type-specific effect on neuronal excitability. Consistent with the role of $Na_V1.2$ in AP generation, *Scn2a* knockdown in olfactory granule cells and heterozygous loss in cerebellar granule cells reduce neuronal spiking activity.[16,22,23] In contrast, homozygous loss of *Scn2a* in cortical pyramidal cells (PCs) and severe knockdown via gene-trap in striatal spiny projection neurons (SPNs) lead to a counterintuitive increase in neuronal excitability.[20,26] At the behavior level, *Scn2a*-haploinsufficient mice exhibit abnormal behaviors such

Please cite this article in press as: Li et al., Selective loss of *Scn2a* in ventral tegmental area dopaminergic neurons leads to dopamine system hypofunction and autistic-like behaviors, Neuron (2025), https://doi.org/10.1016/j.neuron.2025.06.003

as hyperactivity and insufficient anxiety, as well as an increase in social preference that seems contrary to common ASD phenotypes.[27–30] To dissect the mechanism of the pathogenesis, previous studies selectively deleted *Scn2a* from neurons in the medial prefrontal cortex (mPFC), a cortical region involved in social interaction and decision making.[26,31,32] Nonspecific *Scn2a* deletion partially reproduced the behavior manifestations of the haploinsufficient mice, such as the increased preference for social stimuli.[27,29,32] Therefore, the specific brain region and cell type that mediate the core symptoms of ASD associated with *SCN2A* loss of function remain to be explored. Previous immunostaining experiments revealed an expression of $Na_V1.2$ at the axon initial segment (AIS) of midbrain DANs[19]; we therefore focus on the role of $Na_V1.2$ in the control of DAN excitability and ASD-related behaviors.

We show that a selective deletion of *Scn2a* from VTA DANs substantially reduces somatic and axonal Na^+ currents and consequently decreases neuronal excitability and dopamine release at the nucleus accumbens (NAc). In *Scn2a*-heterozygous mice, we also observed reductions in spiking activity of VTA DANs and dopamine release, together with autistic-like behaviors. Importantly, levodopa treatment can rescue the dopamine hypofunction and behavior deficits, suggesting a possible pharmacological treatment for ASD patients with *SCN2A* deficiency and those with dopamine system hypofunction.

RESULTS

$Na_V1.2$ is the prevailing Na^+ channel subtype in VTA DANs

To examine the molecular identity of voltage-dependent Na^+ channels expressed by midbrain DANs, we performed quadruple staining with tyrosine hydroxylase (TH) antibody, DAPI, and RNAscope probes of Na^+ channel isoforms (two at a time, see STAR Methods) in coronal midbrain sections from adult mice (Figures 1A, S1A, and S1B). TH-immunoactive cells were considered as DANs. Among the eight isoforms examined (skeletal muscular *Scn4a* for $Na_V1.4$ was not included), *Scn5a* ($Na_V1.5$, mainly cardiac), *Scn10a* ($Na_V1.8$), and *Scn11a* ($Na_V1.9$) exhibited minimal detectability in VTA DANs, consistent with their predominant expression in the peripheral nervous system. In the rest of the channel isoforms, the expression levels of *Scn2a* and *Scn3a* were much higher than those of other three isoforms (*Scn1a*, *Scn8a*, and *Scn9a*). *Scn2a* showed the strongest positive correlation with the sectional area of the soma among all isoforms, suggesting that *Scn2a* is intensively and widely expressed in DANs (Figures 1B, 1C, and S1C). Positive correlations were also observed in some other channel isoforms, including *Scn8a*, which is strongly expressed by cortical PCs[16,33] but with much fewer particles per cell.

Next, we examined the distribution pattern of $Na_V1.2$ in VTA DANs across developmental stages. Immunostaining of $Na_V1.2$ in neonatal, juvenile, and adult midbrain tissue revealed that $Na_V1.2$ accumulates at the ankyrin-G (AnkG)-labeled AIS (Figure S1D). We then employed the CRISPR-Cas9 strategy to delete *Scn2a* from VTA DANs in 4-week-old mice, allowing examination of the antibody specificity and later the functional roles of $Na_V1.2$. Specifically, we injected an adeno-associated virus (AAV) carrying three different single-guide RNAs targeting mouse *Scn2a* (AAV-*gRNA*-EGFP, Figure 1D) to the left VTA of Dat^{Cre}::$Cas9^{fl}$ mice. In these mice, Cas9 was only expressed by dopamine transporter (*Dat*)-positive neurons (i.e., DANs) labeled by tdTomato. Four weeks after virus injection, we detected $Na_V1.2$ immunosignals at the AIS in the contralateral side but not ipsilateral VTA with virus infection (Figures 1E and 1F). Positive control experiments in mPFC PCs also showed no $Na_V1.2$ immunosignals at the AIS after *Scn2a* deletion in $Thy1^+$ neurons (Figures S2A–S2C).[34]

Scn2a loss reduces excitability and AP propagation

Our experiments revealed hyperexcitability in layer-5 $Thy1^+$ neurons of the mPFC after *Scn2a* deletion (Figures S2D–S2J), in agreement with previous findings.[26] To examine whether similar effects would occur in VTA DANs, we performed whole-cell recordings from $tdTomato^+$/$EGFP^+$ neurons in Dat^{Cre}::$Cas9^{fl}$ mice (Figures 2A–2C). The viruses with *gRNAs* were employed to delete *Scn2a*, whereas those with *gRNAs* omitted (*ΔgRNA*) or scrambled (*scram*) were taken as controls. Neighboring neurons expressing tdTomato alone (i.e., Dat^+ neurons without virus infection) were also recorded as an additional control.

Consistent with previous studies,[35–37] VTA DANs in acute midbrain slices showed spontaneous firing. The average firing frequency and the percentage of cells with spontaneous activity in *gRNA* DANs were significantly lower than those of controls (Figures 2D and 2E). Next, we investigated the contribution of $Na_V1.2$ to neuronal responsiveness to current pulse stimulations. *Scn2a* deletion caused a dramatic reduction in spiking responses (Figures 2F–2H). Surprisingly, we observed a subpopulation of "silent" *gRNA* DANs (17.1%, $n = 82$) in which current pulses (up to 1 nA) could not evoke any AP at −60 mV. APs in *gRNA* DANs showed a substantial increase in voltage threshold but a decrease in peak amplitude (Figures 2I and 2J). *Scn2a* deletion reduced the maximal depolarizing rate of the two AP waveform components, AIS potential and somatodendritic (SD) potential, suggesting an important role of $Na_V1.2$ in AP generation at both compartments (Figures 2I and 2J). In contrast, the AP half-width showed no significant change, and the maximal repolarizing slope was only slightly decreased after *Scn2a* deletion (*gRNA* −73.6 ± 2.7 V/s vs. Dat^+ −84.1 ± 3.4, $p = 0.011$; *gRNA* vs. *scram* −82.7 ± 3.1, $p = 0.033$; *gRNA* vs. *ΔgRNA* −80.4 ± 3.0, $p = 0.059$, Kruskal-Wallis test), suggesting a minor change in voltage-dependent K^+ conductances.

To examine whether the varying degrees of effects result from compensatory expression of other Na_V channel isoforms or incomplete deletion of *Scn2a*, we employed the *Scn2a* floxed mice ($Scn2a^{fl/fl}$) with virus injection (control: AAV-TH-EGFP; cKO: AAV-TH-Cre-EGFP) in VTA to allow selective Cre expression and *Scn2a* conditional knockout (cKO) from Th^+ ($EGFP^+$) cells (Figure S3). Consistent with the low cell specificity of the *Th* promotor,[38] only 44.7% of $EGFP^+$ cells in the VTA were DANs; however, viruses effectively infected the DAN population, with 68.6% of TH-immunopositive DANs co-expressing EGFP (Figures S3A and S3B). We observed a dramatic decrease in *Scn2a* particles, but no significant or minor changes in other Na_V isoforms, suggesting negligible compensation (Figures S3C

Please cite this article in press as: Li et al., Selective loss of *Scn2a* in ventral tegmental area dopaminergic neurons leads to dopamine system hypofunction and autistic-like behaviors, Neuron (2025), https://doi.org/10.1016/j.neuron.2025.06.003

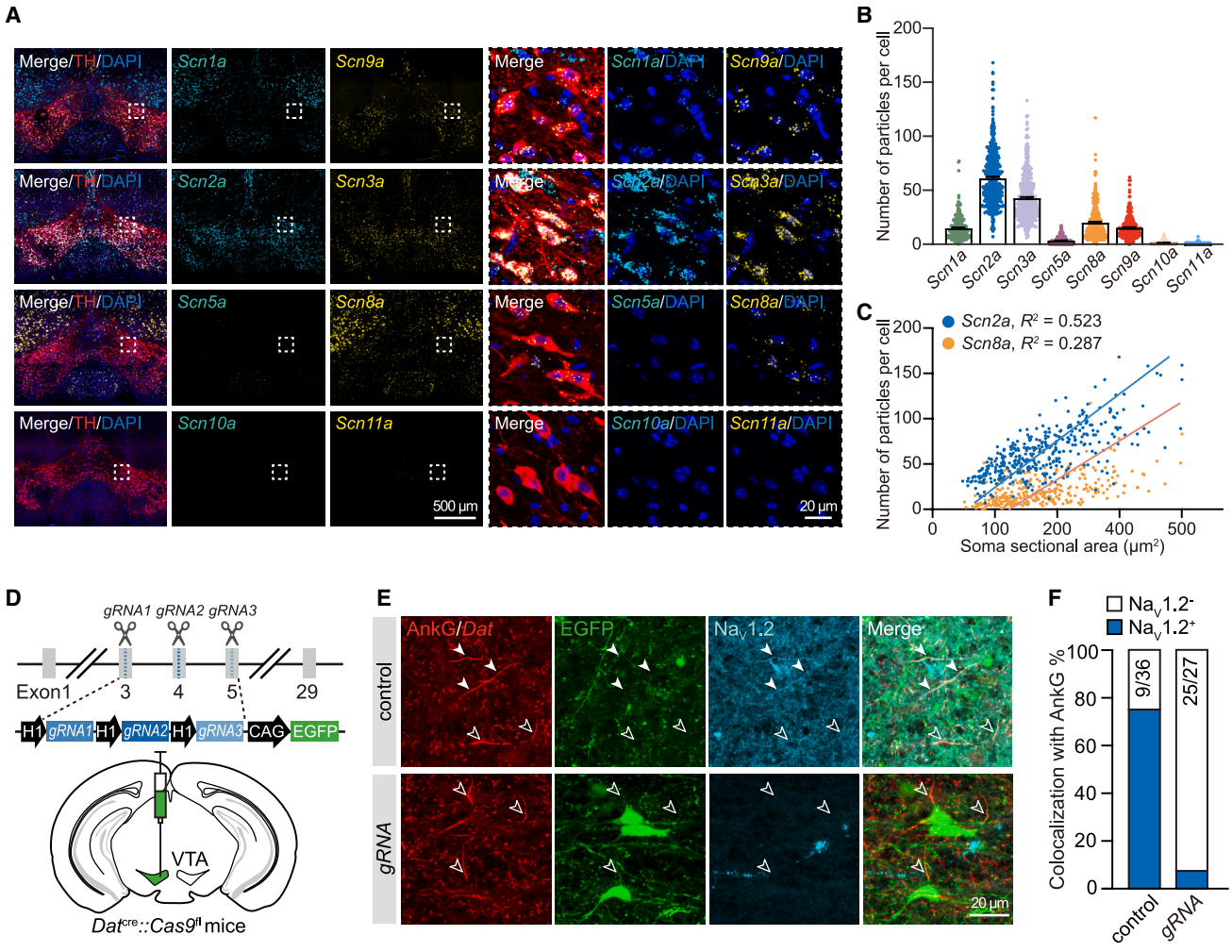

Figure 1. *Scn2a* is the predominant Na_V subtype in VTA DANs

(A) Left, quadruple staining of Na_V isoforms (*in situ* hybridization), TH (immunostaining), and DAPI in WT mouse midbrain sections. Images are shown in single z plane. Right, magnification of the dashed boxes with maximum intensity projection.

(B) Quantification of mRNA particle numbers in TH-positive cells.

(C) Plots of particle numbers versus soma sectional area. Linear regression fits are shown.

(D) Schematic of CRISPR/Cas9-mediated *Scn2a* deletion in VTA *Dat*$^+$ cells. AAV viruses were injected to the left VTA, with the contralateral side serving as a control.

(E) Immunostaining of $Na_V1.2$ and AnkG in VTA sections. White and hollow arrowheads indicate AIS with and without $Na_V1.2$ signals, respectively.

(F) Group data.

For all figures, data are represented as mean ± SEM and the significance levels of statistic comparisons are presented as ns (non-significant) and asterisks (*$p < 0.05$, **$p < 0.01$, ***$p < 0.001$).

See also Figure S1.

and S3D). Whole-cell recording revealed a counterintuitive phenomenon in EGFP$^+$ non-DANs: their spiking responses to large current steps showed an increase rather than a decrease (Figures S3K and S3L). In contrast, *Scn2a*-cKO DANs showed decreases in spiking activity and alterations in AP waveform comparable to those of *gRNA* DANs (Figures S3E–S3J and S4), suggesting a similar loss of *Scn2a* with the two different gene KO strategies. We further sequenced the *gRNA*-targeted region of *Scn2a* using single-cell patch sequencing and observed indels in all examined *gRNA* DANs, with an estimated KO efficiency of 92.3% ($n = 6$, Figure S4A–S4C). Together, these results suggest high gene editing and deletion efficiency of the CRISPR-Cas9 system.

Considering the critical role of *Scn8a* in AP initiation in neocortical PCs[16,18] and its presence in DANs (Figures 1A–1C), we also examined the contribution of *Scn8a* to spontaneous firing and spiking responses in VTA DANs. In *Scn8a* KO (*Scn8a*^{KO}) mice,[39] we found no detectable changes in the spontaneous firing rate, the AP voltage threshold, or waveform, but there was a slight decrease in the frequency of repetitive spiking (Figure S5), suggesting a minor contribution of *Scn8a* to DAN excitability.

Please cite this article in press as: Li et al., Selective loss of *Scn2a* in ventral tegmental area dopaminergic neurons leads to dopamine system hypofunction and autistic-like behaviors, Neuron (2025), https://doi.org/10.1016/j.neuron.2025.06.003

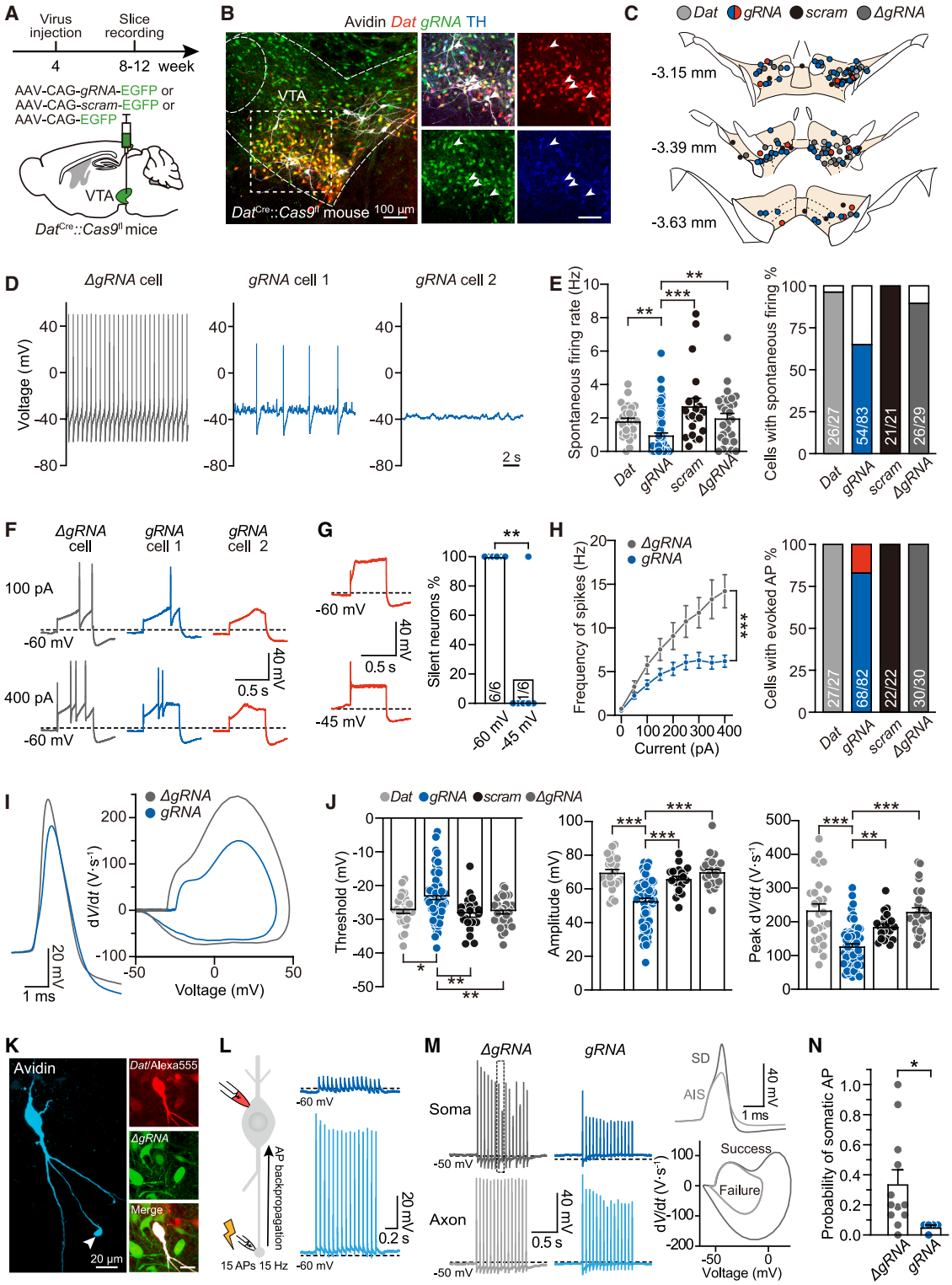

Figure 2. *Scn2a* loss reduces spontaneous firing and alters AP waveform in VTA DANs

(A) Experimental paradigm for *Scn2a* deletion in VTA DANs.

(B) Post hoc staining (avidin and TH-antibody) of recorded EGFP$^+$/tdTomato$^+$ DANs in a coronal VTA slice. Arrowheads denote cells exhibiting quadruple positive fluorescence.

(C) Location of the recorded DANs. Red, *gRNA* DANs without evoked AP.

(legend continued on next page)

Please cite this article in press as: Li et al., Selective loss of *Scn2a* in ventral tegmental area dopaminergic neurons leads to dopamine system hypofunction and autistic-like behaviors, Neuron (2025), https://doi.org/10.1016/j.neuron.2025.06.003

The failure of AP generation in silent DANs may suggest an exclusive expression of *Scn2a*. However, an initial low-amplitude spikelet could be detected (Figures 2F and 2G), possibly due to the activation of somatic A-type K^+ currents that prevents AP backpropagation from the AIS. Indeed, when the membrane potential was depolarized to between −45 and −50 mV to inactivate these K^+ currents,[40,41] most silent neurons could successfully generate the initial AP but still failed to discharge repetitively (Figure 2G). To examine whether *Scn2a* deletion from DANs affects AP conduction along the somato-axonal axis, we next performed dual recordings from the soma and its axonal bleb. In silent neurons at −60 mV, axonal APs could be successfully evoked with axonal stimulation at 15 Hz but could not generate any full APs at the soma (Figures 2K and 2L). For *gRNA* DANs that could generate repetitive somatic APs, we observed AP backpropagation with a reduced probability at a more depolarized membrane potential (Figures 2M and 2N), suggesting a functional segregation between SD and axonal compartments. To investigate the orthodromic conduction of APs, we performed dual recordings from cells with relatively longer axons. Because the background EGFP/tdTomato fluorescence prevents tracing of long axons, we employed *Scn2a*$^{fl/fl}$ mice with AAV-TH-EGFP or AAV-TH-Cre-EGFP injections to VTA (Figure S6), leaving the red channel for axon tracing. Again, the success rate of AP backpropagation was largely reduced at 15 Hz in *Scn2a*-cKO DANs (Figures S6A–S6D). Although APs could faithfully propagate to the axon bleb with somatic stimulation in DANs, the normalized axonal AP amplitude (i.e., axon/soma) was significantly reduced (Figures S6E–S6G).

Together, these results reveal important roles of $Na_V1.2$ in regulating both spontaneous firing and neuronal responsiveness to stimulation. Moreover, $Na_V1.2$ also ensures AP backpropagation and conduction along DAN axons. Loss of $Na_V1.2$ not only reduces spiking activity but also leads to a functional segregation between the SD and axonal compartments.

$Na_V1.2$ contributes significantly to somatic and axonal Na^+ currents

To further examine the distribution of $Na_V1.2$ along the somato-axonal axis of VTA DANs and its contribution to Na^+ currents, we performed patch-clamp recordings from nucleated patches excised from the soma and blebs from the axon, including those formed at the axon trunk in VTA and the axon terminal branches in NAc (Figure 3). In somatic nucleated patches obtained from tdTomato$^+$/EGFP$^+$ DANs of *Dat*^{Cre}::*Cas9*^{fl} mice (Figures 3A–3D), we observed a dramatic reduction of Na^+ currents after *Scn2a* deletion. The peak amplitude in *gRNA* DANs (88.0 ± 16.7 pA, n = 11) was significantly smaller than that in *ΔgRNA* DANs (147.9 ± 21.3, n = 10, p = 0.030, Mann-Whitney test). Calculation of the Na^+ channel density revealed a reduction by 46.1%.

We obtained recordings from isolated axonal blebs to avoid the space clamp problem (Figure 3E, see STAR Methods).[42] In axon-trunk blebs in VTA, a drastic reduction in Na^+ currents was observed in *gRNA* DANs (449 ± 36 pA, n = 9; *ΔgRNA* 1,227 ± 93, n = 8, $p < 0.0001$, unpaired t test; Figures 3F and 3G), reflecting a channel density reduction by 68.7%. No significant change in either the half-activation voltage ($V_{1/2}$) or the slope of activation curve was detected (Figures 3H–3J). Blebs of axon terminal branches in NAc also produced large Na^+ currents, which were significantly reduced after *Scn2a* loss (*ΔgRNA* 729 ± 74 pA, n = 6; *gRNA* 347 ± 57, n = 7, p = 0.002, unpaired t test; Figures 3F and 3G), with a reduction in channel density by 37.3%. Unlike Na^+ currents in the axon trunk, a significant depolarizing shift of the activation $V_{1/2}$ was observed (Figure 3I).

Together, these results show that *Scn2a* deletion dramatically reduces Na^+ currents in VTA DANs. Notably, *Scn2a* deletion causes a much greater reduction of axon-trunk Na^+ currents, which aligns well with the impaired AP conduction along the axon. The residual Na^+ currents observed in both somatic and axonal compartments could be attributable to the activation of other channel subtypes.

Scn2a loss severely decreases dopamine release from DAN axons

The dramatic reduction in Na^+ currents and spiking activity of VTA DANs after *Scn2a* loss may have profound impacts on dopamine release downstream. To detect dopamine signals, we expressed a red fluorescent dopamine sensor rDA3m (D1 receptor based) at the NAc.[43] We employed the *Scn2a*$^{fl/fl}$ mice to leave the red fluorescent channel for dopamine imaging and the green channel for the identification of DANs.

Dopamine release at the axon terminals largely depends on the generation of APs, which can be either the arrival of APs initiated at the AIS or the activation of nicotinic acetylcholine receptors (nAChRs) on axon terminals.[44–46] In coronal NAc slices

(D) Example spontaneous firing.
(E) Group data comparing the rate (left) and the percentage (right) of DANs with spontaneous firing.
(F) Representative voltage responses to 500-ms step current injections (at ∼−60 mV). Note the failure of AP generation in *gRNA* cell 2.
(G) Left, an example silent *gRNA* neuron showing a small spikelet at −60 mV but a full spike at −45 mV. Right, percentages of silent neurons at −60 and −45 mV.
(H) Left, *F-I* curves (two-way ANOVA). Right, percentage of neurons capable or incapable (red) of AP generation.
(I) Superimposed APs evoked at rheobase and their phase plots.
(J) Group data of AP parameters. *Dat*$^+$ n = 27 cells from 9 mice, *gRNA* n = 67 cells from 15 mice, *scram* n = 22 cells from 4 mice, *ΔgRNA* n = 30 cells from 6 mice. Kruskal-Wallis test.
(K) Avidin staining of a recorded EGFP$^+$/tdTomato$^+$ DAN (filled with Alexa Fluor 555 during recording). Arrowhead indicates its axon bleb.
(L) Dual soma-axon recording to examine AP backpropagation toward the somatodendritic (SD) compartment. Right, example voltage responses at −60 mV of a silent *gRNA* neuron to a train of 2-ms pulse stimulation at the bleb.
(M) Left, example dual recordings showing much severe AP backpropagation failure in the *gRNA* DAN. Right, voltage waveforms (dashed box) and their phase plots. Note the waveform difference between the full AP and the spikelet (without SD potential, light gray).
(N) Comparing the probability of the occurrence of full AP at the soma. *ΔgRNA* n = 12 from 4 mice, *gRNA* n = 5 from 2 mice, Mann-Whitney test.
See also Figures S2–S6.

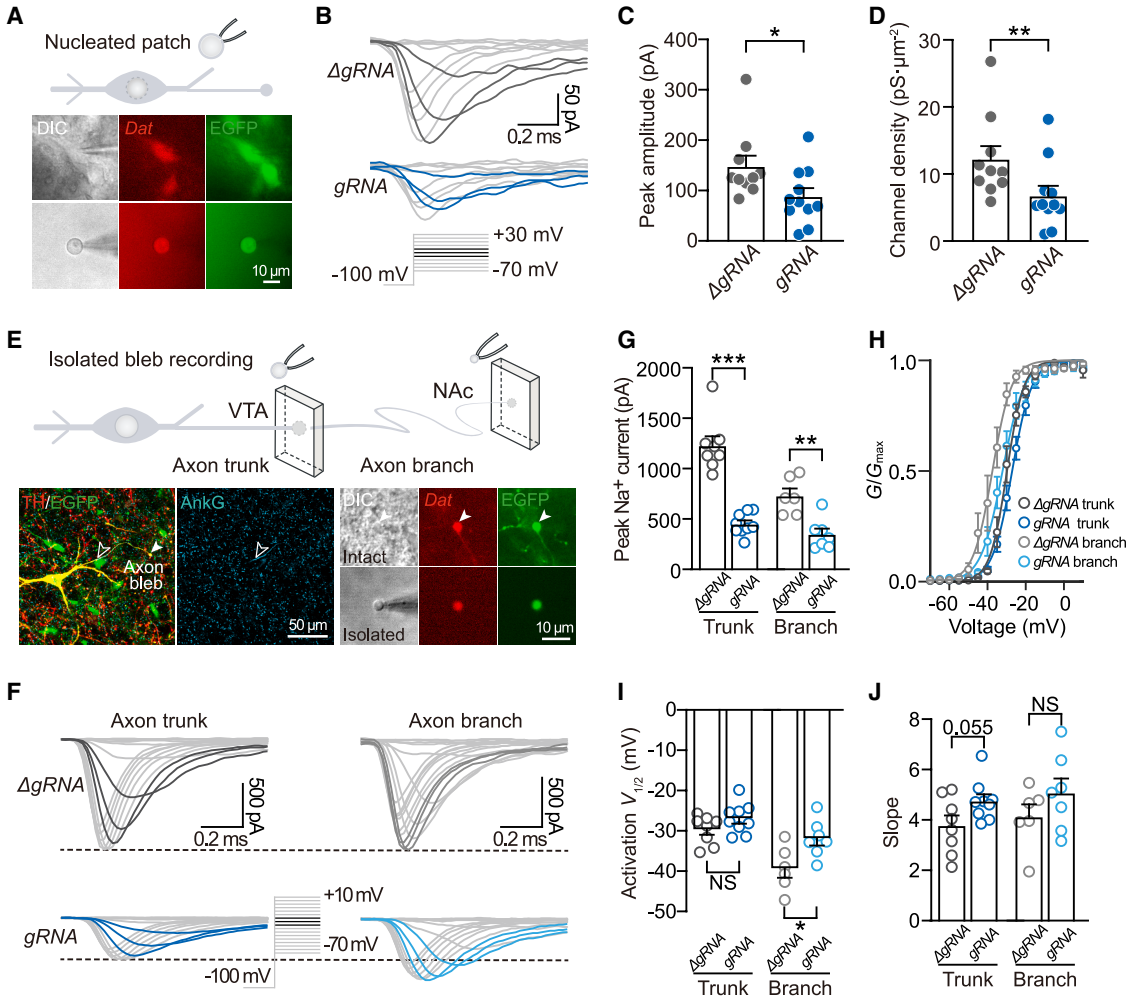

Figure 3. *Scn2a* loss dramatically reduces Na^+ currents along the somato-axonal axis of VTA DANs

(A) Top, schematic of recording from a nucleated patch excised from the soma. Bottom, representative images showing whole-cell recording and nucleated patch recording of an $EGFP^+$/$tdTomato^+$ cell.

(B) Representative families of Na^+ currents from nucleated patches.

(C) Peak amplitude of Na^+ currents obtained from nucleated patches (*ΔgRNA* $n = 10$ from 3 mice, *gRNA* $n = 11$ from 3 mice).

(D) Bar plots of somatic channel density.

(E) Top, schematic of recording from axonal blebs isolated from the axon trunk in VTA or the terminal branch in NAc. Bottom left, confocal images of a TH-positive axonal bleb (white arrowhead) formed near the AIS (hollow arrowhead) in VTA. Bottom right, an axonal bleb in NAc before and after isolation.

(F) Representative families of Na^+ currents obtained from axon-trunk blebs (left) and terminal branch blebs (right).

(G) Quantification of the peak amplitudes of Na^+ currents obtained from trunk blebs (*ΔgRNA* $n = 8$ from 3 mice, *gRNA* $n = 9$ from 2 mice) and terminal branch blebs (control $n = 6$ from 4 mice, 4 *ΔgRNA* blebs, 2 *Dat* blebs; *gRNA* $n = 7$ from 5 mice).

(H) Activation curves of axonal Na^+ currents (fitted with Boltzmann equations).

(I and J) Comparison of the half-activation voltages (I) and the slope factors (J).

containing axon terminals of VTA DANs but without their cell bodies (Figure 4A), we delivered 0.1-ms electric pulses to evoke dopamine release. Changes in rDA3m fluorescence (ΔF) could be detected near the electrode tip and were blocked by the application of D1 receptor selective antagonist SCH39166 (5 μM, Figure 4B). The ratio of ΔF to baseline ($\Delta F/F_0$) was dependent on the stimulation intensity (100–500 μA) and frequency (2–32 Hz at 300 μA) in control (Figures 4C and 4D). In *Scn2a*-cKO slices, we found dramatic reductions in the peak amplitude of $\Delta F/F_0$. We next puffed carbachol (100 μM), a non-selective cholinergic agonist, to NAc slices and found an interesting "popping" phenomenon of momentarily flickering and outwardly spreading rDA3m signals (Figure 4E; Video S1), presumably attributed to the generation and propagation of local APs in DAN axons.[44,47] The amplitude of $\Delta F/F_0$ and the slice area activated by carbachol were significantly reduced in the cKO group (Figures 4F and 4G), suggesting decreased dopamine release and restricted propagation of APs in axon terminal branches.

To confirm the changes of dopamine levels *in vivo*, we performed fiber photometry in freely moving mice. We implanted

Please cite this article in press as: Li et al., Selective loss of *Scn2a* in ventral tegmental area dopaminergic neurons leads to dopamine system hypofunction and autistic-like behaviors, Neuron (2025), https://doi.org/10.1016/j.neuron.2025.06.003

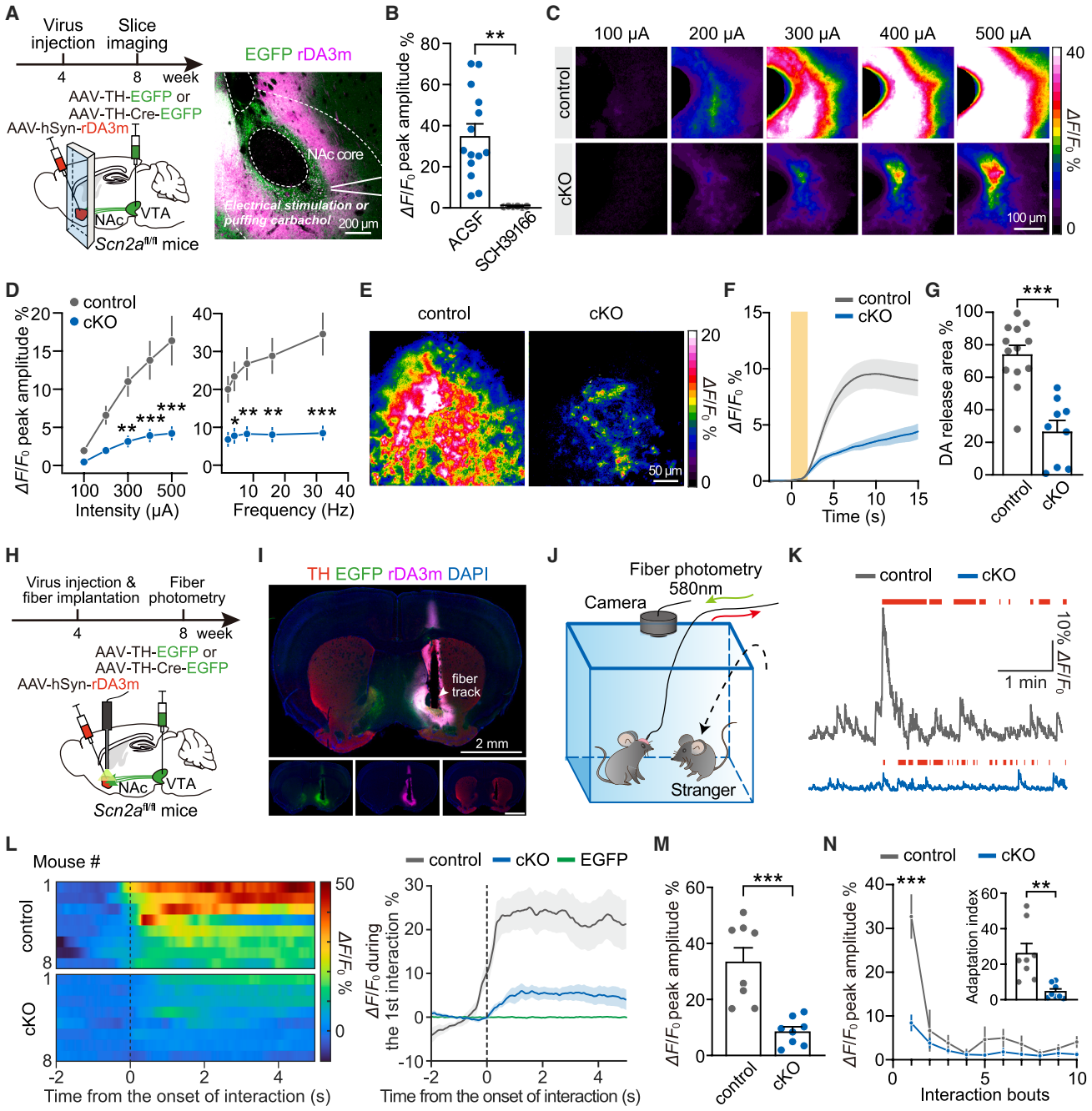

Figure 4. *Scn2a* loss dramatically reduces dopamine release at DAN axon terminals *in vitro* and during social interaction

(A) Left, schematic showing the strategy producing a complete loss of *Scn2a* in VTA DANs of *Scn2a*$^{fl/fl}$ mice and the preparation of NAc slices. Right, an example image showing the expression of EGFP and rDA3m, and the position of an electrical stimulation electrode or a puff pipette (filled with 100 μM carbachol and Alexa Fluor 488) on a NAc slice.

(B) The rDA3m signals evoked by bursts of 0.1-ms electric shocks (300 μA, 32 Hz, 10 pulses) could be completely blocked by bath application of 5 μM SCH39166. Mann-Whitney test.

(C) Example dopamine signals elicited by single electric stimuli at different current intensities.

(D) Dependence of dopamine release on stimulation intensity (left, single electric shocks; control *n* = 17 slices, cKO *n* = 18 slices, 3 mice for each group) and frequency (right, 10-pulse train stimulation with 300 μA; control *n* = 15 slices, cKO *n* = 11 slices, 3 mice for each group). Two-way ANOVA.

(E) Representative images of carbachol-induced dopamine release. Alexa Fluor 488 (100 μM) was added to the puff pipette to visualize drug application.

(F) Quantification of rDA3m fluorescence changes caused by 2-s puffing of carbachol (yellow).

(G) Percentage of the imaged tissue area with rDA3m signal changes induced by carbachol (control *n* = 13 slices, cKO *n* = 9 slices, 3 mice for each group). Unpaired t test.

(legend continued on next page)

Please cite this article in press as: Li et al., Selective loss of *Scn2a* in ventral tegmental area dopaminergic neurons leads to dopamine system hypofunction and autistic-like behaviors, Neuron (2025), https://doi.org/10.1016/j.neuron.2025.06.003

an optical fiber in the NAc core to collect rDA3m fluorescence signals and introduced stranger conspecifics to investigate dopamine release during free social interactions (Figures 4H–4J). Dopamine release during the first social interaction was much less in mice with *Scn2a* loss than that in control (peak amplitude of $\Delta F/F_0$ in control 33.4 ± 5.0%, n = 8; cKO 8.5 ± 1.7%, $n = 8$, $p < 0.0001$, unpaired t test; Figures 4K–4M). In these experiments, we simultaneously recorded EGFP fluorescence as a reference to monitor motion artifacts and found no significant signal changes. The dopamine dynamics during the repeated proactive social investigations also exhibited substantial alterations (Figure 4N). Together, these results suggest that *Scn2a* is indispensable for dopamine secretion from DAN axon terminals.

Scn2a loss in VTA DANs produces repetitive behavior and social deficits

Using the CRISPR-Cas9 strategy, we next examined whether a selective *Scn2a* loss in VTA DANs causes any behavior manifestations associated with ASD (Figure 5A). Injection of *gRNA* viruses affected the majority of VTA regions (75.2 ± 3.0%) but only a small proportion of substantia nigra pars compacta (SNc, 5.8 ± 0.7%, n = 11, Figure 5B). We first monitored the spontaneous behaviors of mice in an open field (see STAR Methods).[48] An increase in the duration of ambulation was observed in *gRNA* mice, accompanied by a trend of reduction in an array of other behaviors, including rearing, jumping, sniffing, and grooming (Figure 5C). Additionally, the traveled distance of these mice was significantly greater than that of control mice, indicative of hyperactivity (Figure 5D). Strikingly, similar to the ASD mouse model with *Fmr1* KO,[49] most *gRNA* mice (n = 9/11) produced repetitive circular locomotion (Figure 5E; Video S2). Each mouse exhibited circular locomotion with a dominant direction, though circling in the opposite direction was also frequently observed (Video S3). Given that the overall percentages of DANs in the left and right VTA were similar, the circling direction may not result from imbalanced virus infection (Figure S7).

Considering that neighboring DANs in SNc also express *Scn2a* (Figure S8A), we further examined whether the locomotion abnormality resulted from virus infection of SNc DANs. We injected *gRNA* viruses into SNc and found dramatic reductions in spiking activity, AP amplitude, and maximal rate of upstroke in SNc DANs (Figures S8B–S8J). However, the mice showed less locomotion and no circling behavior (Figures S8K–S8M). To investigate whether the circular locomotion in *gRNA* mice with *Scn2a* deletion in VTA DANs was associated with increased anxiety,[50–52] we utilized the elevated plus maze test. Distinct from control mice, *gRNA* mice spent a longer time in the open arms (Figure 5F), suggesting an insufficient level of anxiety. The open-arm time ratio showed a positive correlation with the traveled distance (Figure 5G), implying that the hyperactivity was less likely to be resulting from anxiety.

To evaluate changes in social interaction, we introduced a junior stranger mouse into the home cage of the test mouse that had experienced 4 h of social isolation. During the 10-min free investigation, the time of proactive social interaction with the intruder was significantly decreased in *gRNA* mice (Figures 5H and 5I). We also examined social preference in a modified single chamber with two cages (Figure S9A, see STAR Methods). When presented with a choice between a novel object and a novel mouse, *gRNA* mice displayed an even stronger preference for the mouse (the time spent in repetitive actions was omitted; Figure S9B), consistent with the increased social preference in *Scn2a*-haploinsufficient mice.[27,29]

For social novelty preference, we presented the test mouse with a familiar mouse and a stranger mouse in the two cages (Figure 5J). Unlike the control mice, *gRNA* mice spent a similar time near both cages, indicating no preference for social novelty (Figure 5K). Then, we conducted a social novelty recognition test in which a stranger mouse (stranger 1) was repeatedly presented for five trials and then another stranger mouse (stranger 2) in the sixth trial (Figure 5L). Although *gRNA* mice exhibited social habituation during repeated interactions with stranger 1, they failed to recognize and respond actively to stranger 2, with a significant reduction in the social novelty recognition index (Figure 5M).

These results indicate that *Scn2a* deletion from VTA DANs causes hyperactivity and insufficient levels of anxiety. Importantly, mice with *Scn2a* loss from VTA DANs alone show repetitive circular locomotion and impairments of social interaction and social novelty recognition.

Levodopa rescues non-motor deficits in focal *Scn2a*-deletion mice

Next, we performed fiber photometry at the NAc core to examine dopamine dynamics during the social novelty recognition test (Figure S10A). Compared with control mice, dopamine release during the initial proactive social investigation with a stranger was much lower in *gRNA* mice (Figures S10B–S10D). In control mice, we observed a significant decrease in dopamine response to stranger 1 over the repeated trials but an immediate rebound response to stranger 2 (Figures S10E–S10H), in line with their intact social novelty recognition (Figure S10I). However, we detected no significant change in dopamine levels across trials during the whole test in *gRNA* mice (Figure S10G). These results suggest a strong link between social behavior impairments and decreased dopamine levels.

(H) Schematic of selective *Scn2a* deletion from VTA DANs and fiber photometry in NAc in behaving mice.
(I) A coronal section showing the fiber track, dopamine sensor rDA3m expression, EGFP expression, dopaminergic fibers, and DAPI.
(J) Schematic of rDA3m signal recording during free social interaction in an open field.
(K) Representative traces of $\Delta F/F_0$. Red bars represent the bouts of proactive social interactions.
(L) Left, heatmaps of $\Delta F/F_0$ before and after the onset of the first proactive interaction in individual mice. Right, group data. EGFP signals during the recording were taken as a control for the rDA3m signals.
(M) Comparison of the peak $\Delta F/F_0$ amplitude of the first proactive interaction. Unpaired t test.
(N) Peak amplitude of $\Delta F/F_0$ in the first ten bouts of proactive interaction. Two-way ANOVA. Inset, comparing the adaptation index ($\Delta F/F_0$: 1^{st}–2^{nd}). Unpaired t test.

Please cite this article in press as: Li et al., Selective loss of *Scn2a* in ventral tegmental area dopaminergic neurons leads to dopamine system hypofunction and autistic-like behaviors, Neuron (2025), https://doi.org/10.1016/j.neuron.2025.06.003

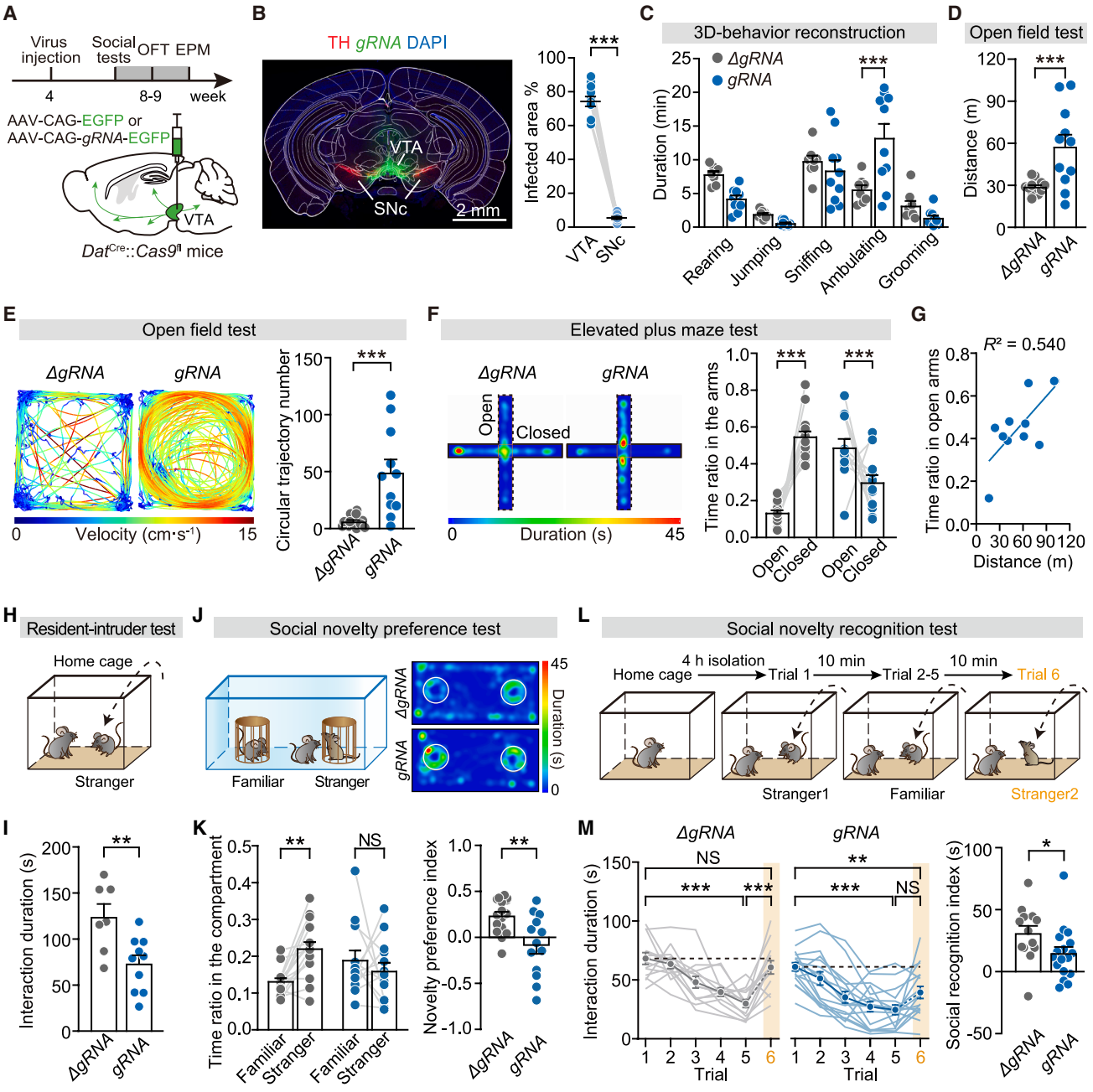

Figure 5. *Scn2a* deletion from VTA DANs causes autistic-like behaviors

(A) Schematic of virus injection and experimental paradigm for behavior tests. OFT, open field test; EPM, elevated plus maze test.

(B) Left, the expression of *gRNA* (EGFP) in a midbrain slice. Right, percentages of infected area in VTA and SNc. Paired t test.

(C) Duration of behavior phenotypes in the 30-min exploration of a novel open field. Two-way ANOVA.

(D) The distance traveled within the first 10 min. Unpaired t test.

(E) Left, representative heatmaps showing the travel trajectory and velocity. Note the apparent circular locomotion of the *gRNA* mouse. Right, comparing the number of circular trajectories. Unpaired t test.

(F) Left, representative heatmaps showing the dwell time spent in different locations. Right, the ratio of time spent in open and closed arms. Two-way ANOVA.

(G) The correlation of the ratio of time spent in the open arms and distance traveled in the open field.

(H) Schematic of free social interaction of the test mouse with a strange mouse.

(I) Total duration of proactive social interactions in (H). Unpaired t test.

(J) Left, schematic of social novelty preference test. Right, representative heatmaps of the dwell time.

(legend continued on next page)

Please cite this article in press as: Li et al., Selective loss of *Scn2a* in ventral tegmental area dopaminergic neurons leads to dopamine system hypofunction and autistic-like behaviors, Neuron (2025), https://doi.org/10.1016/j.neuron.2025.06.003

Inspired by the levodopa treatment for Parkinson's disease that is also attributed to a hypofunction of the dopamine system,[53] we hypothesize that levodopa treatment could be a plausible therapeutic strategy. We first examined the effect of levodopa on dopamine dynamics using opto-stimulation in head-fixed mice (Figures 6A–6D). Dopamine release was evoked by 20 Hz 470-nm light pulses in VTA and monitored by 580 nm light (also 20 Hz) in the NAc core (Figure 6A). We confirmed the efficiency of this optogenetic strategy in acute NAc slices (Figures S11A–S11I). For *in vivo* experiments, levodopa was applied together with benserazide (at quarter mass of levodopa, L/B).[54] We examined the effect of three doses of L/B (5/1.25, 20/5, and 50/12.5 mg·kg^{-1}) on dopamine release to determine an optimal dose. We found a slow but prominent rise of the baseline dopamine signals (Figures 6B and 6C), which should not result from direct binding of levodopa to rDA3m sensors (Figure S11J). Intraperitoneal treatment of SCH23390 (SCH), an antagonist of D1 receptors, abolished the rDA3m signals, confirming a high specificity of the dopamine sensor (Figures S11K and S11L). By analyzing the slow components of the baseline signals, we found that both doses of 20/5 and 50/12.5 mg·kg^{-1} elevated the extracellular dopamine levels in a dose-dependent manner (Figure 6C). In addition, acute intraperitoneal treatment with the modest L/B dose (20/5 mg·kg^{-1}) showed a substantial increase in the rDA3m signals evoked by bursts of light pulses at VTA, which could last for at least 90 min, in *Scn2a*-cKO but not control mice (Figures 6B and 6D). In contrast, saline or a low dose of L/B (5/1.25 mg·kg^{-1}) could not increase dopamine signals. Unexpectedly, the increase in light-evoked rDA3m signals following the high dose (50/12.5 mg·kg^{-1}) was lower than that of the modest dose in cKO mice. With this high dose, there was even a significant decrease in evoked dopamine release in control mice (Figure 6D), possibly due to self-inhibition mediated by over-activation of D2 autoreceptors.[55] We therefore chose the dose of 20/5 mg·kg^{-1} to examine whether L/B treatment could rescue behavior deficits in focal *Scn2a* deletion mice.

The *Dat*^{Cre}::*Cas9*^{fl} mice underwent a series of consecutive behavior tests 5 weeks after the virus injection to VTA (Figure 6E). On the day of tests, mice received a single dose of saline or 20/5 mg·kg^{-1} L/B (counterbalanced) and behavior assessments within 10 to 60 min after the intraperitoneal injection. We found that L/B treatment showed no obvious relief of the hyperactivity or circular locomotion (Figure 6F) but alleviated the non-motor behavior deficits in *gRNA* mice. L/B treatment significantly reduced the preference for the open arms to a control level (Figure 6G). In addition, the social preference (Figure S9C) and the social novelty preference (Figure 6H) were improved to control levels, and the social novelty recognition was restored, as reflected by the rebound of interest to a novel stranger (Figure 6I). Together, the results indicate that levodopa treatment with an appropriate dose increases dopamine release and rescues non-motor behavior deficits in mice with focal *Scn2a* loss in VTA DANs.

Levodopa shows therapeutic effects in *Scn2a*-heterozygous mice

We next employed more disease-relevant heterozygous (*Scn2a*$^{+/-}$) mice to examine whether they also show autistic-like behavior and dopamine system hypofunction and whether behavior deficits could be rescued by L/B treatment. These heterozygous mice carried one normal copy of the *Scn2a* gene and one copy with a deletion of exons 4-6 (Figure 7A). Similar to a recent study,[23] we also observed hypersensitive sensorimotor reflexes in these mice during handling in the behavior tests.

As compared with wild-type (WT; *Scn2a*$^{+/+}$) mice, *Scn2a*$^{+/-}$ mice exhibited hyperactivity (but without repetitive circular locomotion) and insufficient anxiety levels, similar to *gRNA* mice (Figures 7B and 7C). In addition, *Scn2a*$^{+/-}$ mice also showed severe deficits in sociability, as indicated by an excessive preference of a mouse over an object (Figure S12A), a significant reduction in the total duration of proactive social interactions with the intruder (resident-intruder test, Figure 7D), a substantial decrease in capability of distinguishing between the familiar and the stranger mouse in the social novelty preference test (Figure 7E), and a lack of rebound interest to the second stranger in the social novelty recognition test (Figure 7F).

We next treated the WT and *Scn2a*$^{+/-}$ mice with an intraperitoneal injection of saline or 20/5 mg·kg^{-1} L/B to examine their behavior changes. Most likely due to hypersensitivity of *Scn2a*$^{+/-}$ mice in response to noxious injections,[23] both saline and L/B treatment reduced their traveled distance in the open field test (Figure S12C). For non-motor behaviors, L/B rescued the insufficient anxiety and sociability impairments of *Scn2a*$^{+/-}$ mice, whereas saline showed no significant effect (Figures 7G–7I and S12). Specifically, L/B significantly decreased the time spent in open arms, increased the preference to the stranger mouse in the social novelty preference test, and produced a dramatic rebound interest to stranger 2 in the social novelty recognition test. Remarkably, L/B treatment rescued these behavior deficits of *Scn2a*$^{+/-}$ mice to a level similar to control, indicating a potent therapeutic effect of levodopa.

The effect of levodopa also suggests hypofunction of the dopamine system in *Scn2a*$^{+/-}$ mice. Indeed, similar to *gRNA* mice, dopamine release in *Scn2a*$^{+/-}$ mice during the initial proactive social interactions with stranger 1 in the first 5 trials was substantially less than that of WT mice (p = 0.019, two-way ANOVA), and the release associated with stranger 2 showed no rebound in *Scn2a*$^{+/-}$ mice (Figure 8A). After these experiments, we examined the basal dopamine release through intraperitoneal treatment of 6 mg·kg^{-1} SCH and found that *Scn2a*$^{+/-}$ mice exhibited much lower basal levels than WT mice (Figures 8B and 8C, see STAR Methods). Our electrophysiological results from VTA DANs of the heterozygous mice

(K) Comparison of the time ratio in each compartment (left, two-way ANOVA) and the social novelty preference index (right, unpaired t test).
(L) Schematic of social novelty recognition test. The stranger 1 was introduced repeatedly from trial 1–5, and the stranger 2 was introduced in trial 6.
(M) The duration of proactive interactions in different trials (left, two-way ANOVA) and the social recognition index (right, unpaired t test).
See also Figures S7–S9.

Please cite this article in press as: Li et al., Selective loss of *Scn2a* in ventral tegmental area dopaminergic neurons leads to dopamine system hypofunction and autistic-like behaviors, Neuron (2025), https://doi.org/10.1016/j.neuron.2025.06.003

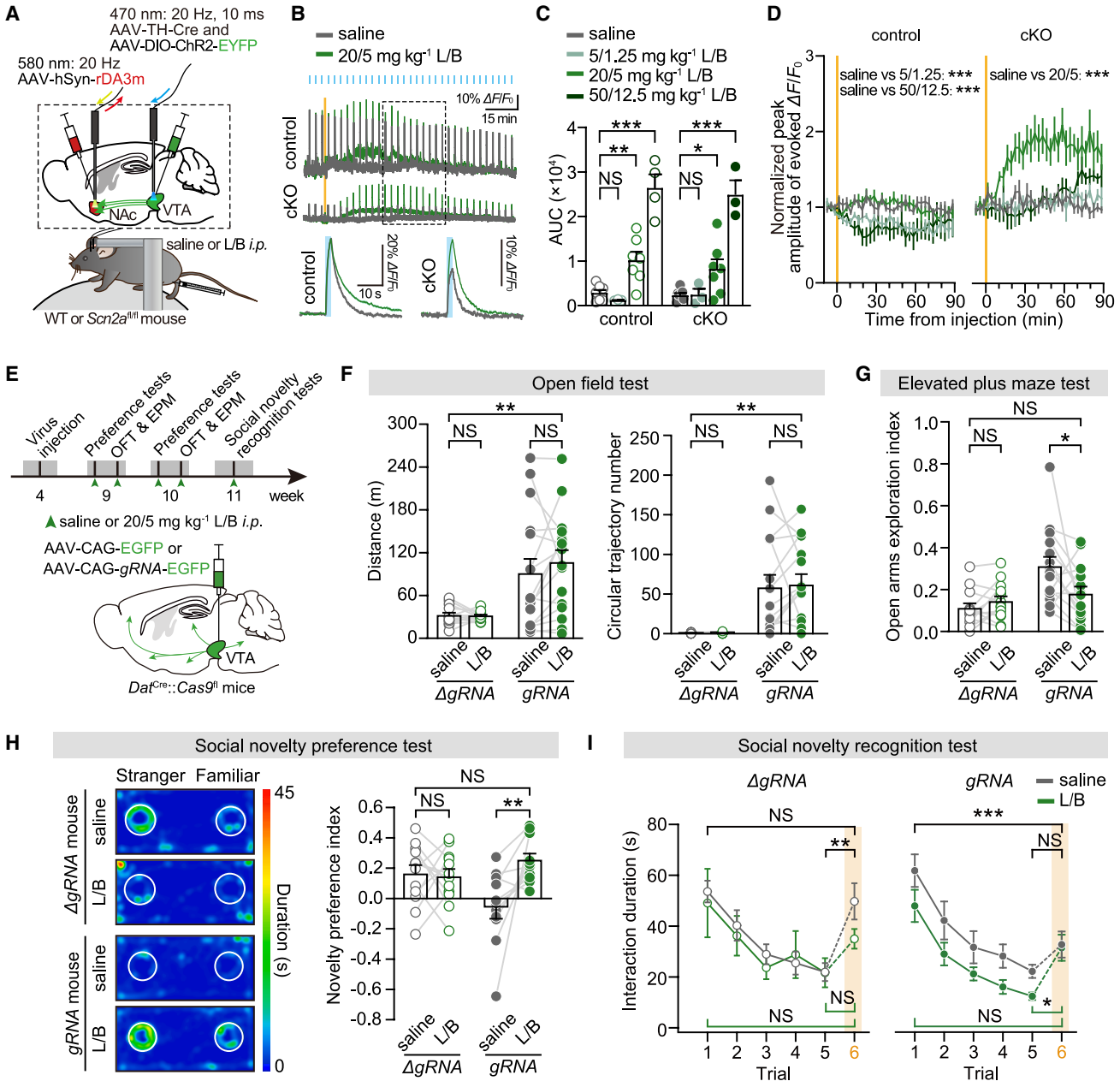

Figure 6. Acute treatment of levodopa rescues social behavior deficits and insufficient anxiety

(A) Schematic of virus injections that allow the expression of rDA3m sensors in NAc core and ChR2 in VTA *Th*$^{+}$ neurons of *Scn2a*$^{fl/fl}$ mice. The optic fiber implanted at NAc core was used for monitoring dopamine release and the optic fiber at VTA for optogenetic activation in head-fixed mice.

(B) Top, example traces showing rDA3m signals before and after intraperitoneal application of saline or 20/5 mg·kg^{-1}L/B (yellow bar). Note the slow increase of the baseline rDA3m signal after L/B treatment (green traces) in both control and cKO mice. The thick and noisy baseline of rDA3m fluorescence reflects barrages of dopamine release events in control mice. Bottom, averaged traces of the evoked rDA3m signals in the dashed box were overlaid for comparison.

(C) Comparison of the slow increase of the baseline fluorescence signal at different doses of L/B. The slow baseline increase of rDA3m signal was quantified by calculating the area under the curve (AUC) over a period of 90 min after saline or L/B injection. Two-way ANOVA.

(D) Changes in transient rDA3m signals evoked by optogenetic stimulation with intraperitoneal injection of different doses of L/B (yellow bars). Data were normalized to each mouse's average release level prior to injection. Two-way ANOVA.

(E) Schematic of virus injection and experimental paradigm for behavior tests after intraperitoneal injection of saline or 20/5 mg·kg^{-1}L/B.

(F) Comparison of the distance traveled (left) and the number of circular trajectories (right). Two-way ANOVA.

(G) Comparison of the open arms exploration index. Two-way ANOVA.

(legend continued on next page)

Please cite this article in press as: Li et al., Selective loss of *Scn2a* in ventral tegmental area dopaminergic neurons leads to dopamine system hypofunction and autistic-like behaviors, Neuron (2025), https://doi.org/10.1016/j.neuron.2025.06.003

showed reductions in the spontaneous firing rate and the proportion of cells with spontaneous activity (Figures 8D–8G) as well as decreases in spiking responsiveness to current injections (Figures 8H and 8I). Although the voltage threshold remained unchanged, we found significant reductions in the peak amplitude and the maximal rate of AP upstroke (Figures 8J and 8K).

Together, these results suggest that the downregulated spiking activity of VTA DANs may lead to reduced basal and behavior-associated dopamine release, contributing to the autistic-like behaviors observed in *Scn2a*$^{+/-}$ mice. Importantly, the potent therapeutic effect of levodopa in alleviating non-motor behavior deficits of *Scn2a*$^{+/-}$ mice highlights a possible pharmacological treatment strategy for individuals with *SCN2A* loss-of-function mutations.

DISCUSSION

Distinct from previous findings showing paradoxical hyperexcitability of neocortical PCs and striatal SPNs with a severe loss of *Scn2a*,[20,26] our results reveal a dramatic hypo-excitability in *Scn2a*-deleted DANs and even complete failure of AP generation. Given the high KO efficiency of *Scn2a* achieved with *gRNA*s (Figure S4) and the minor compensatory contributions from less abundant Na_V subtypes (Figures S3C and S3D), the varying degrees of reduction in spiking activity reflect heterogeneous expression levels of $Na_V1.2$ across individual DANs. Whether those with high $Na_V1.2$ expression represent a distinct cell subpopulation with specific circuit functions remains to be further examined.

Dopamine can be secreted from both axon terminals and SD compartments.[56,57] The substantial contributions of $Na_V1.2$ to somatic and axonal Na^+ currents suggest a crucial role of this channel isoform in AP-dependent dopamine release from both compartments. Consistent with a recent study that found terminal release relies on the arrival of propagating axonal APs or locally initiated APs by the activation of nAChR,[44] our experiments in NAc slices demonstrate that the loss of *Scn2a* largely reduces both modes of release (Figures 4A–4G). In agreement with our findings, intracellular application of $Na_V1.2$ antibody decreased spiking activity of SNc DANs and reduced the inhibitory postsynaptic currents mediated by D2 autoreceptors,[58] suggesting a contribution of $Na_V1.2$ to dopamine release at the SD compartments.

ASD individuals with *SCN2A* mutations tend to exhibit various repetitive actions and limited sociability in initiating or responding to social interactions.[30] We observed several autistic-like behaviors in *Scn2a*-heterozygous mice, including insufficient anxiety level and deficits in social novelty (Figure 7). These pronounced behavioral impairments contrast with previous reports that showed minor trends or no apparent effects, possibly attributable to differences in methodology and gene mutation.[18,59,60] For example, we prolonged the interval between the social preference and novelty tests, which may produce difficulties in memorizing the social cues. Indeed, we observed social memory deficits in the social recognition test, consistent with impaired hippocampal-dependent memory in *Scn2a*-haploinsufficient mice.[28,61,62] Mice with *Scn2a* deletion specifically in VTA DANs recapture these phenotypes observed in *Scn2a*-heterozygous mice (Figure 5), suggesting a critical role of VTA DANs in the pathogenesis of ASD with *SCN2A* loss of function. Previous studies also revealed the involvement of VTA DANs in these manifestations.[9,63] Consistent with our findings, genetic inhibition of VTA DANs reduces social interactions, social novelty preference, and anxiety levels,[7,9,10,64] and mild lesions of VTA DANs lead to increased spontaneous locomotion.[65] However, some behavior deficits induced by focal *Scn2a* deletion weakly correlate with or are even seemingly contradictory to the known functions of VTA DANs. First, the repetitive circular locomotion has not been associated with activities of VTA neurons in previous studies. Second, the increased social preference seems contrary to previous findings, where reducing activity of VTA DANs diminishes social preference.[6] Finally, the hyperactivity observed in mice with focal *Scn2a* loss could also be induced by activating VTA DANs.[50] These contradictory findings could be attributable to heterogenous expression levels of *Scn2a* in DANs (Figures 1B, 2E, and 2H), with distinct projections contributing to different behaviors.[52,66–70] The dissociation of spiking activity in SD and axon compartments (Figures 2K–2N and S6) could be another explanation for the differences between our observations and those with universal suppression of DAN activity.

Dopamine system hypofunction has been observed in both ASD patients and mouse models.[3–6,8,71,72] However, a recent study revealed that mice with a nonspecific deletion of *Scn2a* from VTA neurons exhibit no obvious autistic-like behaviors.[32] It may be attributed to simultaneous dysfunction of DANs and other types of VTA neurons. Indeed, *Scn2a* mRNA was also detected in VTA TH-immunonegative neurons (Figure 1A), where *Scn2a* deletion led to a counterintuitive increase in neuronal spiking responses to strong inputs (Figures S3K and S3L). Unlike the nonspecific manipulation, a selective loss of *Scn2a* from VTA DANs produces autistic-like behaviors, providing strong evidence that the hypofunction of the dopamine system may be a common pathway of ASD pathogenesis. Interestingly, an early study showed that low-dose levodopa treatment has no clear overall effect but yielded improvements in 20% of autistic children.[73] The responsive individuals might be those with dopamine system hypofunction. The modest dose of levodopa in our experiments may exert its effect through simultaneous increases in phasic firings of DANs and dopamine release in target regions.[74,75] Its rescue results agree with previous findings that elevating dopamine release in NAc by phasic opto-activation facilitates sociability and social novelty preference.[7,10] Recent studies also showed that the dopamine replacement treatment could ameliorate social impairments in rodents with aberrant midbrain structures, including DAN loss.[76,77]

(H) Left, representative heatmaps of dwell time from the same mouse after injection of saline or 20 mg·kg^{-1} L/B. Right, social novelty preference index of *gRNA* mice is significantly increased to a control level with L/B treatment. Two-way ANOVA.
(I) Averaged total duration of proactive interaction (Δ*gRNA*, saline $n = 9$, L/B $n = 6$; *gRNA*, saline $n = 8$, L/B $n = 9$). Two-way ANOVA.
See also Figures S10 and S11.

Please cite this article in press as: Li et al., Selective loss of *Scn2a* in ventral tegmental area dopaminergic neurons leads to dopamine system hypofunction and autistic-like behaviors, Neuron (2025), https://doi.org/10.1016/j.neuron.2025.06.003

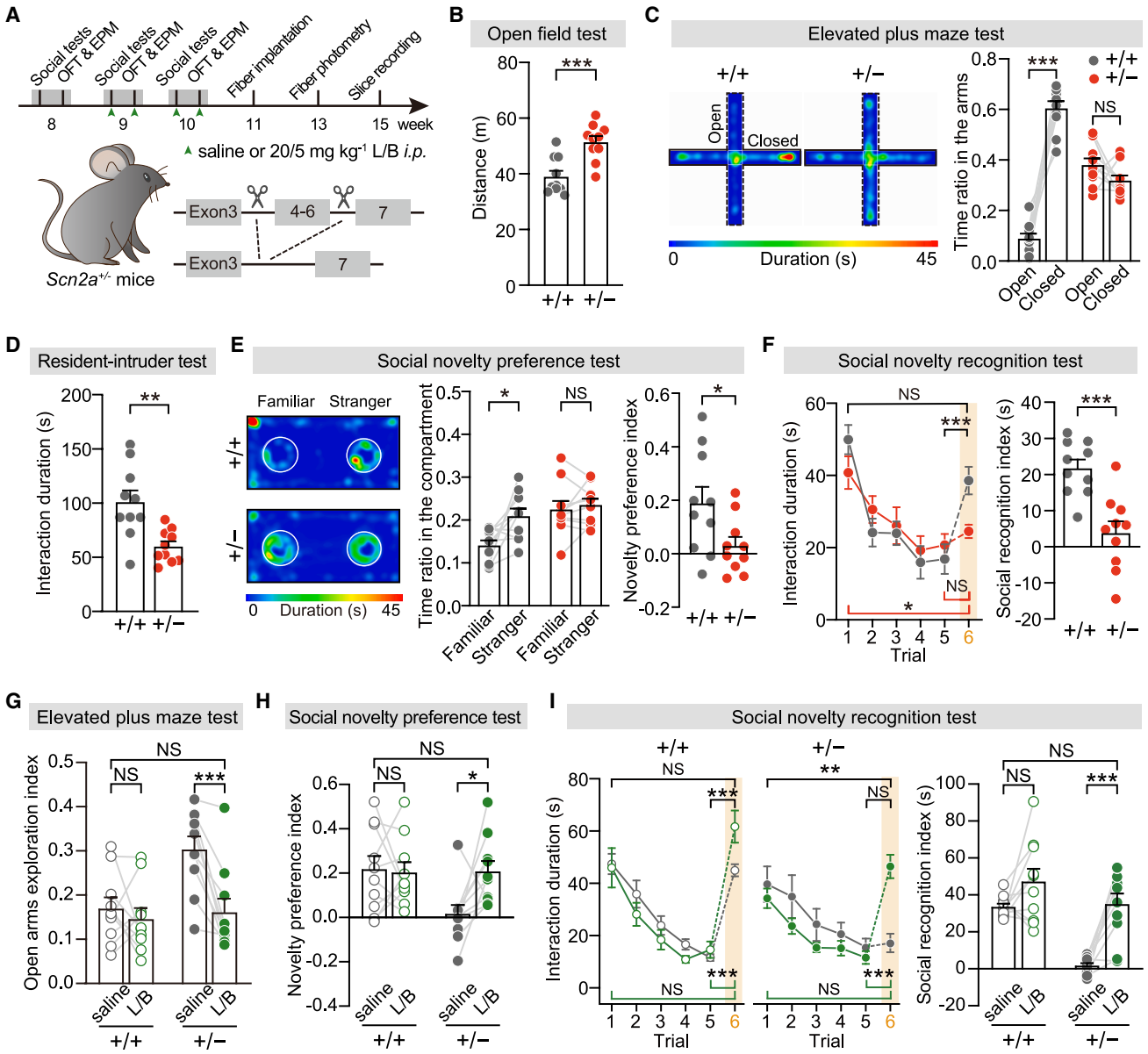

Figure 7. *Scn2a*-heterozygous mice exhibit autistic-like behaviors that can be alleviated by L/B treatment

(A) Schematic illustrating the deletion site of *Scn2a* gene for generating the heterozygous mouse line, and the experimental timeline for WT ($Scn2a^{+/+}$) and $Scn2a^{+/-}$ mice. Each mouse received either saline or L/B injection, with a randomized and counterbalanced order.

(B) Distance traveled in open field test. Mann-Whitney test.

(C) Left, representative heatmaps showing spatial exploration patterns. Right, group data comparing the ratios of time spent in open or closed arms to the total time of the test. Two-way ANOVA.

(D) Comparison of total time engaged in proactive social interactions. Unpaired t test.

(E) Left, representative heatmaps of dwell time around a familiar or a stranger mouse. Middle, group data comparing the ratios of time spent in the two different compartments. Two-way ANOVA. Right, comparison of the social novelty preference index. Unpaired t test.

(F) Left, plots of the duration of proactive social interactions in the social novelty recognition test. Two-way ANOVA. Right, comparison of the social novelty recognition index. Unpaired t test.

(G) Group data comparing the open arms exploration index after the injection of saline or L/B. Two-way ANOVA.

(H) Comparison of the social novelty preference index after drug injection. Two-way ANOVA.

(I) Left, average duration of proactive social interactions in each trial. Two-way ANOVA. Right, comparison of the social recognition index. Two-way ANOVA.

See also Figure S12.

Please cite this article in press as: Li et al., Selective loss of *Scn2a* in ventral tegmental area dopaminergic neurons leads to dopamine system hypofunction and autistic-like behaviors, Neuron (2025), https://doi.org/10.1016/j.neuron.2025.06.003

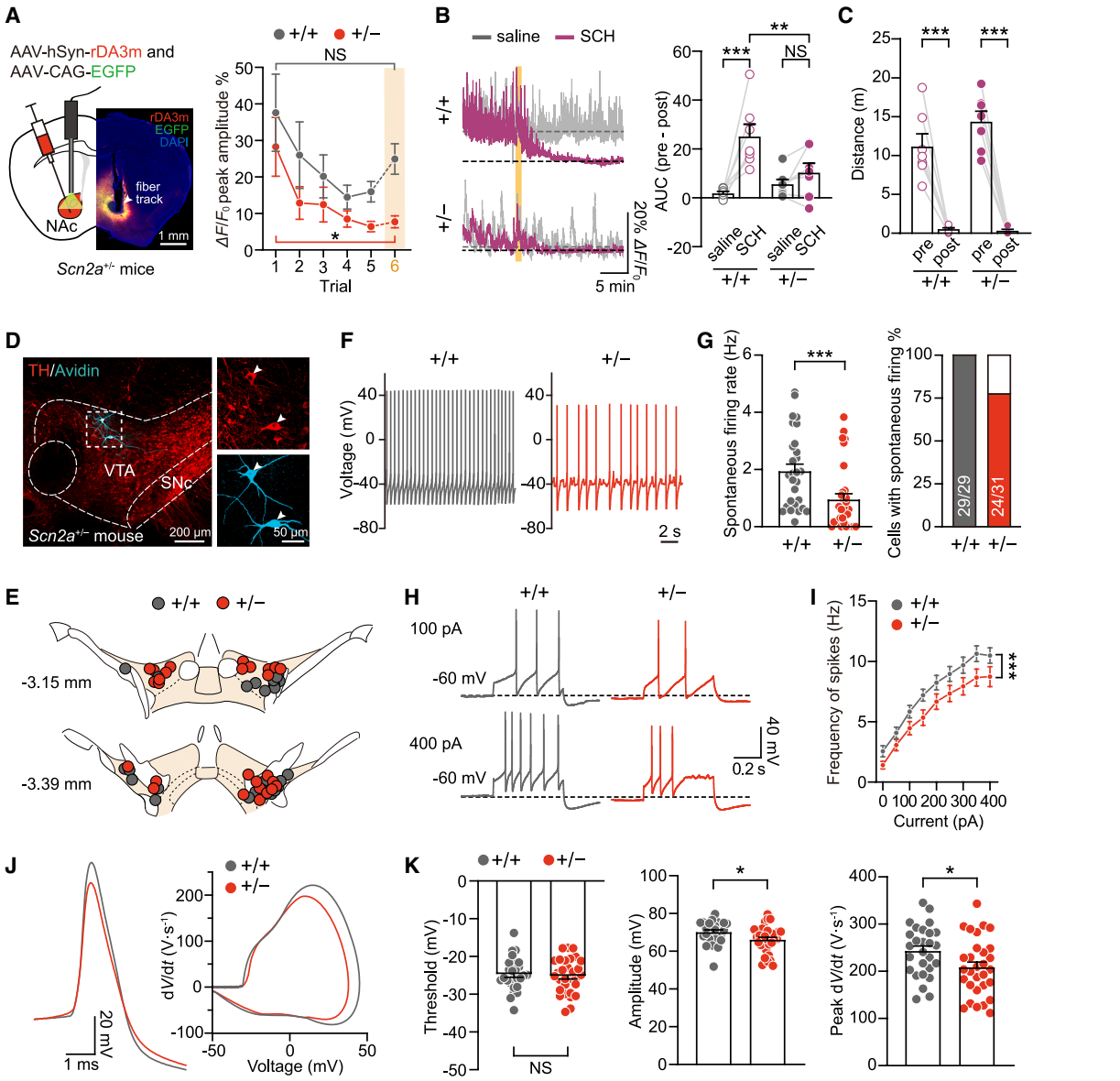

Figure 8. Dopamine release and spiking activity of VTA DANs are substantially reduced in *Scn2a* heterozygous mice

(A) Left, schematic of fiber photometry and a representative image of a fiber track in NAc. Right, average peak $\Delta F/F_0$ amplitude of rDA3m signals in NAc core during the initial investigation of the stranger in social novelty recognition test. Two-way ANOVA.

(B) Left, representative traces of rDA3m signals during spontaneous locomotion in the open field and after saline or 6 mg·kg^{-1} SCH application (yellow bar) in WT and *Scn2a*$^{+/-}$ mice. Right, difference in AUC within 5 min before (pre) and 15 min after (post) saline or SCH injection. Dashed lines, F_0 was calculated as the average fluorescence intensity from 10 to 20 min post injection (see Methods). Two-way ANOVA.

(C) Distance traveled before and after SCH treatment. WT n = 7 mice, *Scn2a*$^{+/-}$ n = 7 mice, two-way ANOVA.

(D) Confocal images showing recorded neurons with avidin and TH staining (arrowheads) in a coronal VTA section.

(E) Location of recorded cells revealed by avidin staining.

(F) Example traces of spontaneous firing of DANs.

(G) Group data of spontaneous firing rates and cell percentages.

(H) Representative voltage responses of DANs to 500-ms step current injections.

(I) *F-I* curves. Two-way ANOVA.

(J) Superimposed APs evoked at rheobase and their phase plots.

(K) Group data of AP parameters (WT n = 27 from 3 mice, *Scn2a*$^{+/-}$ n = 30 from 3 mice). Unpaired t test.

In our experiments, we found that levodopa treatment increased ambient dopamine concentrations in both control and *Scn2a*-cKO mice. Interestingly, we also observed that levodopa enhanced optogenetically evoked dopamine release, but this effect was specific to *Scn2a*-cKO mice and only occurred at a modest dose. A possible explanation for these different effects could be the activation of D2 autoreceptors distributed at DAN axons. In control mice, levodopa raises dopamine levels to a concentration above the physiological range, which would activate D2 receptors and thus suppress AP-evoked dopamine release. In *Scn2a* deletion mice, a moderate dose of levodopa restores dopamine to a near-physiological level, but a higher dose may not further increase dopamine release due to D2 receptor activation. Interestingly, levodopa treatment produced no effect on hyperactivity and circular locomotion in the *gRNA*-expressing mice, suggesting a potential contribution from other neurotransmitters (glutamate or gamma-aminobutyric acid [GABA]) co-released from DAN axons.[66,78] The similarity of repetitive circular locomotion between *gRNA* mice and *Fmr1*^{KO} mice or *MECP2*-overexpressing monkeys[49,79] suggests that *Scn2a* might be a downstream target of these corresponding genes or other transcription regulators and chromatin modifiers.[80] Whether this results from a severe loss of *Scn2a* from DANs, and thereby a hypofunction of dopamine system in these autism models, remains to be further examined.

RESOURCE AVAILABILITY

Lead contact

Requests for further information and resources should be directed to, and will be fulfilled by, the lead contact, Yousheng Shu (yousheng@fudan.edu.cn).

Materials availability

This study did not generate new unique reagents. Materials including mouse lines and viruses are commercially available.

Data and code availability

- All data reported in this paper will be shared by the lead contact upon request.
- Original code has been deposited at Zenodo (https://doi.org/10.5281/zenodo.15597751) and is publicly available as of the date of publication.
- Any additional information required to reanalyze the data reported in this paper is available from the lead contact upon request.

ACKNOWLEDGMENTS

We are grateful to Drs. Minghu Han, Zilong Qiu, Man Jiang, and Rongfeng Hu for valuable comments and suggestions on experiments. This study was supported by National Natural Science Foundation of China (NSFC) (32130044 and T2241002, Y.S.), Ministry of Science and Technology of China (STI2030-Major Projects 2021ZD0202500, Y.S.), and Program of Shanghai Academic/Technology Research Leader (21XD1400100, Y.S.), as well as NSFC grants (32200951, Y.X.; 32100930, Q. He; and 32200953, W.K.) and China Postdoctoral Science Foundation (2022M720801, Y.X.).

AUTHOR CONTRIBUTIONS

Conceptualization, Y.S., L.L., and Q. Huang; methodology, Y.S., Y.L., W.W., B. L., Y.T., J. He, and T.-l.C.; investigation, L.L., Q. Huang, W.K., Y.Z., Y.X., M.J., and X.Z.; formal analysis, L.L., Q. Huang, J. Hu, Q. He, and W.K.; writing of original draft, Y.S., L.L., and Q. Huang; review and editing, Y.S., F.G., and J.Y.; visualization, Y.S., L.L., Q. Huang, and J. Hu; supervision, Y.S.; funding acquisition, Y.S., Y.X., Q. He, and W.K.

DECLARATION OF INTERESTS

The authors declare no competing interests.

STAR★METHODS

Detailed methods are provided in the online version of this paper and include the following:

- KEY RESOURCES TABLE
- EXPERIMENTAL MODEL AND STUDY PARTICIPANT DETAILS
- METHOD DETAILS
  - Fluorescent *in situ* hybridization
  - Stereotaxic surgeries
  - Imaging dopamine release in brain slices
  - Behavior tests
  - *In vivo* levodopa treatment
  - Fiber photometry of dopamine release
  - *In vivo* optogenetic stimulation
- QUANTIFICATION AND STATISTICAL ANALYSIS

SUPPLEMENTAL INFORMATION

Supplemental information can be found online at https://doi.org/10.1016/j.neuron.2025.06.003.

Received: June 11, 2024
Revised: February 21, 2025
Accepted: June 5, 2025

REFERENCES

1. Landa, R.J. (2008). Diagnosis of autism spectrum disorders in the first 3 years of life. Nat. Clin. Pract. Neurol. *4*, 138–147. https://doi.org/10.1038/ncpneuro0731.
2. Willsey, H.R., Willsey, A.J., Wang, B., and State, M.W. (2022). Genomics, convergent neuroscience and progress in understanding autism spectrum disorder. Nat. Rev. Neurosci. *23*, 323–341. https://doi.org/10.1038/s41583-022-00576-7.
3. Ernst, M., Zametkin, A.J., Matochik, J.A., Pascualvaca, D., and Cohen, R. M. (1997). Low medial prefrontal dopaminergic activity in autistic children. Lancet *350*, 638. https://doi.org/10.1016/s0140-6736(05)63326-0.
4. Saha, S., Chatterjee, M., Dutta, N., Sinha, S., and Mukhopadhyay, K. (2023). Analysis of neurotransmitters validates the importance of the dopaminergic system in autism spectrum disorder. World J. Pediatr. *19*, 770–781. https://doi.org/10.1007/s12519-023-00702-0.
5. Supekar, K., Kochalka, J., Schaer, M., Wakeman, H., Qin, S., Padmanabhan, A., and Menon, V. (2018). Deficits in mesolimbic reward pathway underlie social interaction impairments in children with autism. Brain *141*, 2795–2805. https://doi.org/10.1093/brain/awy191.
6. Bariselli, S., Tzanoulinou, S., Glangetas, C., Prévost-Solié, C., Pucci, L., Viguié, J., Bezzi, P., O'Connor, E.C., Georges, F., Lüscher, C., and Bellone, C. (2016). SHANK3 controls maturation of social reward circuits in the VTA. Nat. Neurosci. *19*, 926–934. https://doi.org/10.1038/nn.4319.
7. Bariselli, S., Hörnberg, H., Prévost-Solié, C., Musardo, S., Hatstatt-Burklé, L., Scheiffele, P., and Bellone, C. (2018). Role of VTA dopamine neurons and neuroligin 3 in sociability traits related to nonfamiliar conspecific interaction. Nat. Commun. *9*, 3173. https://doi.org/10.1038/s41467-018-05382-3.
8. Hörnberg, H., Pérez-Garci, E., Schreiner, D., Hatstatt-Burklé, L., Magara, F., Baudouin, S., Matter, A., Nacro, K., Pecho-Vrieseling, E., and Scheiffele, P. (2020). Rescue of oxytocin response and social behaviour

in a mouse model of autism. Nature *584*, 252–256. https://doi.org/10.1038/s41586-020-2563-7.

9. Gunaydin, L.A., Grosenick, L., Finkelstein, J.C., Kauvar, I.V., Fenno, L.E., Adhikari, A., Lammel, S., Mirzabekov, J.J., Airan, R.D., Zalocusky, K.A., et al. (2014). Natural neural projection dynamics underlying social behavior. Cell *157*, 1535–1551. https://doi.org/10.1016/j.cell.2014.05.017.
10. Dai, B., Sun, F., Tong, X., Ding, Y., Kuang, A., Osakada, T., Li, Y., and Lin, D. (2022). Responses and functions of dopamine in nucleus accumbens core during social behaviors. Cell Rep. *40*, 111246. https://doi.org/10.1016/j.celrep.2022.111246.
11. Sanders, S.J., Murtha, M.T., Gupta, A.R., Murdoch, J.D., Raubeson, M.J., Willsey, A.J., Ercan-Sencicek, A.G., DiLullo, N.M., Parikshak, N.N., Stein, J.L., et al. (2012). De novo mutations revealed by whole-exome sequencing are strongly associated with autism. Nature *485*, 237–241. https://doi.org/10.1038/nature10945.
12. Trost, B., Thiruvahindrapuram, B., Chan, A.J.S., Engchuan, W., Higginbotham, E.J., Howe, J.L., Loureiro, L.O., Reuter, M.S., Roshandel, D., Whitney, J., et al. (2022). Genomic architecture of autism from comprehensive whole-genome sequence annotation. Cell *185*, 4409–4427.e18. https://doi.org/10.1016/j.cell.2022.10.009.
13. Satterstrom, F.K., Kosmicki, J.A., Wang, J., Breen, M.S., De Rubeis, S., An, J.Y., Peng, M., Collins, R., Grove, J., Klei, L., et al. (2020). Large-scale exome sequencing study implicates both developmental and functional changes in the neurobiology of autism. Cell *180*, 568–584.e23. https://doi.org/10.1016/j.cell.2019.12.036.
14. Zhou, X., Feliciano, P., Shu, C., Wang, T., Astrovskaya, I., Hall, J.B., Obiajulu, J.U., Wright, J.R., Murali, S.C., Xu, S.X., et al. (2022). Integrating de novo and inherited variants in 42,607 autism cases identifies mutations in new moderate-risk genes. Nat. Genet. *54*, 1305–1319. https://doi.org/10.1038/s41588-022-01148-2.
15. De Rubeis, S., He, X., Goldberg, A.P., Poultney, C.S., Samocha, K., Cicek, A.E., Kou, Y., Liu, L., Fromer, M., Walker, S., et al. (2014). Synaptic, transcriptional and chromatin genes disrupted in autism. Nature *515*, 209–215. https://doi.org/10.1038/nature13772.
16. Hu, W., Tian, C., Li, T., Yang, M., Hou, H., and Shu, Y. (2009). Distinct contributions of Na(v)1.6 and Na(v)1.2 in action potential initiation and backpropagation. Nat. Neurosci. *12*, 996–1002. https://doi.org/10.1038/nn.2359.
17. Li, T., Tian, C., Scalmani, P., Frassoni, C., Mantegazza, M., Wang, Y., Yang, M., Wu, S., and Shu, Y. (2014). Action potential initiation in neocortical inhibitory interneurons. PLoS Biol. *12*, e1001944. https://doi.org/10.1371/journal.pbio.1001944.
18. Spratt, P.W.E., Ben-Shalom, R., Keeshen, C.M., Burke, K.J., Jr., Clarkson, R.L., Sanders, S.J., and Bender, K.J. (2019). The autism-associated gene Scn2a contributes to dendritic excitability and synaptic function in the prefrontal cortex. Neuron *103*, 673–685.e5. https://doi.org/10.1016/j.neuron.2019.05.037.
19. Yang, J., Xiao, Y., Li, L., He, Q., Li, M., and Shu, Y. (2019). Biophysical properties of somatic and axonal voltage-gated sodium channels in midbrain dopaminergic neurons. Front. Cell. Neurosci. *13*, 317. https://doi.org/10.3389/fncel.2019.00317.
20. Zhang, J., Chen, X., Eaton, M., Wu, J., Ma, Z., Lai, S., Park, A., Ahmad, T. S., Que, Z., Lee, J.H., et al. (2021). Severe deficiency of the voltage-gated sodium channel NaV1.2 elevates neuronal excitability in adult mice. Cell Rep. *36*, 109495. https://doi.org/10.1016/j.celrep.2021.109495.
21. Yamagata, T., Ogiwara, I., Mazaki, E., Yanagawa, Y., and Yamakawa, K. (2017). Nav1.2 is expressed in caudal ganglionic eminence-derived disinhibitory interneurons: Mutually exclusive distributions of Nav1.1 and Nav1.2. Biochem. Biophys. Res. Commun. *491*, 1070–1076. https://doi.org/10.1016/j.bbrc.2017.08.013.
22. Nunes, D., and Kuner, T. (2018). Axonal sodium channel NaV1.2 drives granule cell dendritic GABA release and rapid odor discrimination. PLoS Biol. *16*, e2003816. https://doi.org/10.1371/journal.pbio.2003816.
23. Wang, C., Derderian, K.D., Hamada, E., Zhou, X., Nelson, A.D., Kyoung, H., Ahituv, N., Bouvier, G., and Bender, K.J. (2024). Impaired cerebellar plasticity hypersensitizes sensory reflexes in SCN2A-associated ASD. Neuron *112*, 1444–1455.e5. https://doi.org/10.1016/j.neuron.2024.01.029.
24. Ben-Shalom, R., Keeshen, C.M., Berrios, K.N., An, J.Y., Sanders, S.J., and Bender, K.J. (2017). Opposing effects on NaV1.2 function underlie differences between SCN2A variants observed in individuals with autism spectrum disorder or infantile seizures. Biol. Psychiatry *82*, 224–232. https://doi.org/10.1016/j.biopsych.2017.01.009.
25. Begemann, A., Acuña, M.A., Zweier, M., Vincent, M., Steindl, K., Bachmann-Gagescu, R., Hackenberg, A., Abela, L., Plecko, B., Kroell-Seger, J., et al. (2019). Further corroboration of distinct functional features in SCN2A variants causing intellectual disability or epileptic phenotypes. Mol. Med. *25*, 6. https://doi.org/10.1186/s10020-019-0073-6.
26. Spratt, P.W.E., Alexander, R.P.D., Ben-Shalom, R., Sahagun, A., Kyoung, H., Keeshen, C.M., Sanders, S.J., and Bender, K.J. (2021). Paradoxical hyperexcitability from NaV1.2 sodium channel loss in neocortical pyramidal cells. Cell Rep. *36*, 109483. https://doi.org/10.1016/j.celrep.2021.109483.
27. Tatsukawa, T., Raveau, M., Ogiwara, I., Hattori, S., Miyamoto, H., Mazaki, E., Itohara, S., Miyakawa, T., Montal, M., and Yamakawa, K. (2019). Scn2a haploinsufficient mice display a spectrum of phenotypes affecting anxiety, sociability, memory flexibility and ampakine CX516 rescues their hyperactivity. Mol. Autism *10*, 15. https://doi.org/10.1186/s13229-019-0265-5.
28. Shin, W., Kweon, H., Kang, R., Kim, D., Kim, K., Kang, M., Kim, S.Y., Hwang, S.N., Kim, J.Y., Yang, E., et al. (2019). Scn2a haploinsufficiency in mice suppresses hippocampal neuronal excitability, excitatory synaptic drive, and long-term potentiation, and spatial learning and memory. Front. Mol. Neurosci. *12*, 145. https://doi.org/10.3389/fnmol.2019.00145.
29. Wang, H.G., Bavley, C.C., Li, A., Jones, R.M., Hackett, J., Bayleyen, Y., Lee, F.S., Rajadhyaksha, A.M., and Pitt, G.S. (2021). Scn2a severe hypomorphic mutation decreases excitatory synaptic input and causes autism-associated behaviors. JCI Insight *6*, e150698. https://doi.org/10.1172/jci.insight.150698.
30. Sanders, S.J., Campbell, A.J., Cottrell, J.R., Moller, R.S., Wagner, F.F., Auldridge, A.L., Bernier, R.A., Catterall, W.A., Chung, W.K., Empfield, J. R., et al. (2018). Progress in understanding and treating SCN2A-mediated disorders. Trends Neurosci. *41*, 442–456. https://doi.org/10.1016/j.tins.2018.03.011.
31. Chini, M., and Hanganu-Opatz, I.L. (2021). Prefrontal cortex development in health and disease: lessons from rodents and humans. Trends Neurosci. *44*, 227–240. https://doi.org/10.1016/j.tins.2020.10.017.
32. Suzuki, T., Hattori, S., Mizukami, H., Nakajima, R., Hibi, Y., Kato, S., Matsuzaki, M., Ikebe, R., Miyakawa, T., and Yamakawa, K. (2024). Inversed effects of Nav1.2 deficiency at medial prefrontal cortex and ventral tegmental area for prepulse inhibition in acoustic startle response. Mol. Neurobiol. *61*, 622–634. https://doi.org/10.1007/s12035-023-03610-6.
33. Liao, Y., Deprez, L., Maljevic, S., Pitsch, J., Claes, L., Hristova, D., Jordanova, A., Ala-Mello, S., Bellan-Koch, A., Blazevic, D., et al. (2010). Molecular correlates of age-dependent seizures in an inherited neonatal-infantile epilepsy. Brain *133*, 1403–1414. https://doi.org/10.1093/brain/awq057.
34. Dewachter, I., Reversé, D., Caluwaerts, N., Ris, L., Kuipéri, C., Van den Haute, C., Spittaels, K., Umans, L., Serneels, L., Thiry, E., et al. (2002). Neuronal deficiency of presenilin 1 inhibits amyloid plaque formation and corrects hippocampal long-term potentiation but not a cognitive defect of amyloid precursor protein [V717I] transgenic mice. J. Neurosci. *22*, 3445–3453. https://doi.org/10.1523/JNEUROSCI.22-09-03445.2002.
35. Liss, B., Franz, O., Sewing, S., Bruns, R., Neuhoff, H., and Roeper, J. (2001). Tuning pacemaker frequency of individual dopaminergic neurons by Kv4.3L and KChip3.1 transcription. EMBO J. *20*, 5715–5724. https://doi.org/10.1093/emboj/20.20.5715.

36. Khaliq, Z.M., and Bean, B.P. (2008). Dynamic, nonlinear feedback regulation of slow pacemaking by A-type potassium current in ventral tegmental area neurons. J. Neurosci. *28*, 10905–10917. https://doi.org/10.1523/JNEUROSCI.2237-08.2008.

37. Chieng, B., Azriel, Y., Mohammadi, S., and Christie, M.J. (2011). Distinct cellular properties of identified dopaminergic and GABAergic neurons in the mouse ventral tegmental area. J. Physiol. *589*, 3775–3787. https://doi.org/10.1113/jphysiol.2011.210807.

38. Lammel, S., Steinberg, E.E., Földy, C., Wall, N.R., Beier, K., Luo, L., and Malenka, R.C. (2015). Diversity of transgenic mouse models for selective targeting of midbrain dopamine neurons. Neuron *85*, 429–438. https://doi.org/10.1016/j.neuron.2014.12.036.

39. Burgess, D.L., Kohrman, D.C., Galt, J., Plummer, N.W., Jones, J.M., Spear, B., and Meisler, M.H. (1995). Mutation of a new sodium channel gene, Scn8a, in the mouse mutant 'motor endplate disease'. Nat. Genet. *10*, 461–465. https://doi.org/10.1038/ng0895-461.

40. Gentet, L.J., and Williams, S.R. (2007). Dopamine gates action potential backpropagation in midbrain dopaminergic neurons. J. Neurosci. *27*, 1892–1901. https://doi.org/10.1523/JNEUROSCI.5234-06.2007.

41. Koyama, S., and Appel, S.B. (2006). A-type K+ current of dopamine and GABA neurons in the ventral tegmental area. J. Neurophysiol. *96*, 544–554. https://doi.org/10.1152/jn.01318.2005.

42. Shu, Y., Hasenstaub, A., Duque, A., Yu, Y., and McCormick, D.A. (2006). Modulation of intracortical synaptic potentials by presynaptic somatic membrane potential. Nature *441*, 761–765. https://doi.org/10.1038/nature04720.

43. Zhuo, Y., Luo, B., Yi, X., Dong, H., Miao, X., Wan, J., Williams, J.T., Campbell, M.G., Cai, R., Qian, T., et al. (2024). Improved green and red GRAB sensors for monitoring dopaminergic activity in vivo. Nat. Methods *21*, 680–691. https://doi.org/10.1038/s41592-023-02100-w.

44. Liu, C., Cai, X., Ritzau-Jost, A., Kramer, P.F., Li, Y., Khaliq, Z.M., Hallermann, S., and Kaeser, P.S. (2022). An action potential initiation mechanism in distal axons for the control of dopamine release. Science *375*, 1378–1385. https://doi.org/10.1126/science.abn0532.

45. Zhou, F.M., Liang, Y., and Dani, J.A. (2001). Endogenous nicotinic cholinergic activity regulates dopamine release in the striatum. Nat. Neurosci. *4*, 1224–1229. https://doi.org/10.1038/nn769.

46. Zhang, H., and Sulzer, D. (2004). Frequency-dependent modulation of dopamine release by nicotine. Nat. Neurosci. *7*, 581–582. https://doi.org/10.1038/nn1243.

47. Kramer, P.F., Brill-Weil, S.G., Cummins, A.C., Zhang, R., Camacho-Hernandez, G.A., Newman, A.H., Eldridge, M.A.G., Averbeck, B.B., and Khaliq, Z.M. (2022). Synaptic-like axo-axonal transmission from striatal cholinergic interneurons onto dopaminergic fibers. Neuron *110*, 2949–2960.e4. https://doi.org/10.1016/j.neuron.2022.07.011.

48. Huang, K., Han, Y., Chen, K., Pan, H., Zhao, G., Yi, W., Li, X., Liu, S., Wei, P., and Wang, L. (2021). A hierarchical 3D-motion learning framework for animal spontaneous behavior mapping. Nat. Commun. *12*, 2784. https://doi.org/10.1038/s41467-021-22970-y.

49. Dolan, B.M., Duron, S.G., Campbell, D.A., Vollrath, B., Shankaranarayana Rao, B.S., Ko, H.Y., Lin, G.G., Govindarajan, A., Choi, S.Y., and Tonegawa, S. (2013). Rescue of fragile X syndrome phenotypes in Fmr1 KO mice by the small-molecule PAK inhibitor FRAX486. Proc. Natl. Acad. Sci. USA *110*, 5671–5676. https://doi.org/10.1073/pnas.1219383110.

50. Tong, Q., Cui, X., Xu, H., Zhang, X., Hu, S., Huang, F., and Xiao, L. (2023). D1 receptor-expressing neurons in ventral tegmental area alleviate mouse anxiety-like behaviors via glutamatergic projection to lateral septum. Mol. Psychiatry *28*, 625–638. https://doi.org/10.1038/s41380-022-01809-y.

51. Morel, C., Montgomery, S.E., Li, L., Durand-de Cuttoli, R., Teichman, E.M., Juarez, B., Tzavaras, N., Ku, S.M., Flanigan, M.E., Cai, M., et al. (2022). Midbrain projection to the basolateral amygdala encodes anxiety-like but not depression-like behaviors. Nat. Commun. *13*, 1532. https://doi.org/10.1038/s41467-022-29155-1.

52. Nguyen, C., Mondoloni, S., Le Borgne, T., Centeno, I., Come, M., Jehl, J., Solié, C., Reynolds, L.M., Durand-de Cuttoli, R., Tolu, S., et al. (2021). Nicotine inhibits the VTA-to-amygdala dopamine pathway to promote anxiety. Neuron *109*, 2604–2615.e9. https://doi.org/10.1016/j.neuron.2021.06.013.

53. Fahn, S. (2008). The history of dopamine and levodopa in the treatment of Parkinson's disease. Mov. Disord. *23*, S497–S508. https://doi.org/10.1002/mds.22028.

54. Rinne, U.K., Birket-Smith, E., Dupont, E., Hansen, E., Hyyppä, M., Marttila, R., Mikkelsen, B., Pakkenberg, H., and Presthus, J. (1975). Levodopa alone and in combination with a peripheral decarboxylase inhibitor benserazide (Madopar) in the treatment of Parkinson's disease: A controlled clinical trial. J. Neurol. *211*, 1–9. https://doi.org/10.1007/BF00312459.

55. Ford, C.P. (2014). The role of D2-autoreceptors in regulating dopamine neuron activity and transmission. Neuroscience *282*, 13–22. https://doi.org/10.1016/j.neuroscience.2014.01.025.

56. Rice, M.E., and Patel, J.C. (2015). Somatodendritic dopamine release: recent mechanistic insights. Philos. Trans. R. Soc. Lond. B Biol. Sci. *370*, 20140185. https://doi.org/10.1098/rstb.2014.0185.

57. Liu, C., Goel, P., and Kaeser, P.S. (2021). Spatial and temporal scales of dopamine transmission. Nat. Rev. Neurosci. *22*, 345–358. https://doi.org/10.1038/s41583-021-00455-7.

58. Hikima, T., Lee, C.R., Witkovsky, P., Chesler, J., Ichtchenko, K., and Rice, M.E. (2021). Activity-dependent somatodendritic dopamine release in the substantia nigra autoinhibits the releasing neuron. Cell Rep. *35*, 108951. https://doi.org/10.1016/j.celrep.2021.108951.

59. Echevarria-Cooper, D.M., Hawkins, N.A., Misra, S.N., Huffman, A.M., Thaxton, T., Thompson, C.H., Ben-Shalom, R., Nelson, A.D., Lipkin, A.M., George, A.L., Jr., et al. (2022). Cellular and behavioral effects of altered NaV1.2 sodium channel ion permeability in Scn2aK1422E mice. Hum. Mol. Genet. *31*, 2964–2988. https://doi.org/10.1093/hmg/ddac087.

60. Léna, I., and Mantegazza, M. (2019). Na(V)1.2 haploinsufficiency in Scn2a knock-out mice causes an autistic-like phenotype attenuated with age. Sci. Rep. *9*, 12886. https://doi.org/10.1038/s41598-019-49392-7.

61. Middleton, S.J., Kneller, E.M., Chen, S., Ogiwara, I., Montal, M., Yamakawa, K., and McHugh, T.J. (2018). Altered hippocampal replay is associated with memory impairment in mice heterozygous for the Scn2a gene. Nat. Neurosci. *21*, 996–1003. https://doi.org/10.1038/s41593-018-0163-8.

62. Keith, R.E., Shen, Y., Janzen-Meza, J.A., Abramovitz, J., Antonello, P.C., Hameed, A., Mohana Krishnan, B., and Antoine, M.W. (2025). Perirhinal cortex abnormalities impair hippocampal plasticity and learning in Scn2a, Fmr1, and Cdkl5 autism mouse models. Sci. Adv. *11*, eadt0780. https://doi.org/10.1126/sciadv.adt0780.

63. Bromberg-Martin, E.S., Matsumoto, M., and Hikosaka, O. (2010). Dopamine in motivational control: rewarding, aversive, and alerting. Neuron *68*, 815–834. https://doi.org/10.1016/j.neuron.2010.11.022.

64. Qi, G., Zhang, P., Li, T., Li, M., Zhang, Q., He, F., Zhang, L., Cai, H., Lv, X., Qiao, H., et al. (2022). NAc-VTA circuit underlies emotional stress-induced anxiety-like behavior in the three-chamber vicarious social defeat stress mouse model. Nat. Commun. *13*, 577. https://doi.org/10.1038/s41467-022-28190-2.

65. Koob, G.F., Stinus, L., and Le Moal, M. (1981). Hyperactivity and hypoactivity produced by lesions to the mesolimbic dopamine system. Behav. Brain Res. *3*, 341–359. https://doi.org/10.1016/0166-4328(81)90004-8.

66. Morales, M., and Margolis, E.B. (2017). Ventral tegmental area: cellular heterogeneity, connectivity and behaviour. Nat. Rev. Neurosci. *18*, 73–85. https://doi.org/10.1038/nrn.2016.165.

67. Garritsen, O., van Battum, E.Y., Grossouw, L.M., and Pasterkamp, R.J. (2023). Development, wiring and function of dopamine neuron subtypes. Nat. Rev. Neurosci. *24*, 134–152. https://doi.org/10.1038/s41583-022-00669-3.

68. Poulin, J.F., Caronia, G., Hofer, C., Cui, Q., Helm, B., Ramakrishnan, C., Chan, C.S., Dombeck, D.A., Deisseroth, K., and Awatramani, R. (2018). Mapping projections of molecularly defined dopamine neuron subtypes using intersectional genetic approaches. Nat. Neurosci. *21*, 1260–1271. https://doi.org/10.1038/s41593-018-0203-4.

69. Wu, M., Zhang, X., Feng, S., Freda, S.N., Kumari, P., Dumrongprechachan, V., and Kozorovitskiy, Y. (2024). Dopamine pathways mediating affective state transitions after sleep loss. Neuron *112*, 141–154.e8. https://doi.org/10.1016/j.neuron.2023.10.002.

70. Beier, K.T., Steinberg, E.E., DeLoach, K.E., Xie, S., Miyamichi, K., Schwarz, L., Gao, X.J., Kremer, E.J., Malenka, R.C., and Luo, L. (2015). Circuit architecture of VTA dopamine neurons revealed by systematic input-output mapping. Cell *162*, 622–634. https://doi.org/10.1016/j.cell.2015.07.015.

71. Scott-Van Zeeland, A.A., Dapretto, M., Ghahremani, D.G., Poldrack, R.A., and Bookheimer, S.Y. (2010). Reward processing in autism. Autism Res. *3*, 53–67. https://doi.org/10.1002/aur.122.

72. Bowton, E., Saunders, C., Reddy, I.A., Campbell, N.G., Hamilton, P.J., Henry, L.K., Coon, H., Sakrikar, D., Veenstra-VanderWeele, J.M., Blakely, R.D., et al. (2014). SLC6A3 coding variant Ala559Val found in two autism probands alters dopamine transporter function and trafficking. Transl. Psychiatry *4*, e464. https://doi.org/10.1038/tp.2014.90.

73. Sugiyama, N., Sugie, H., Igarashi, Y., Ito, M., and Fukuda, T. (1998). Low-dose levodopa therapy of autistic disorder: evaluation of clinical effectiveness. No To Hattatsu *30*, 51–55.

74. Paladini, C.A., Robinson, S., Morikawa, H., Williams, J.T., and Palmiter, R. D. (2003). Dopamine controls the firing pattern of dopamine neurons via a network feedback mechanism. Proc. Natl. Acad. Sci. USA *100*, 2866–2871. https://doi.org/10.1073/pnas.0138018100.

75. Koshimura, K., Ohue, T., Akiyama, Y., Itoh, A., and Miwa, S. (1992). L-dopa administration enhances exocytotic dopamine release in vivo in the rat striatum. Life Sci. *51*, 747–755. https://doi.org/10.1016/0024-3205(92)90484-7.

76. Chao, O.Y., Pathak, S.S., Zhang, H., Dunaway, N., Li, J.S., Mattern, C., Nikolaus, S., Huston, J.P., and Yang, Y.M. (2020). Altered dopaminergic pathways and therapeutic effects of intranasal dopamine in two distinct mouse models of autism. Mol. Brain *13*, 111. https://doi.org/10.1186/s13041-020-00649-7.

77. Li, Y., Zhu, M., Chen, W.X., Luo, J., Li, X., Cao, Y., Zheng, M., Ma, S., Xiao, Z., Zhang, Y., et al. (2023). A novel mutation in intron 1 of Wnt1 causes developmental loss of dopaminergic neurons in midbrain and ASD-like behaviors in rats. Mol. Psychiatry *28*, 3795–3805. https://doi.org/10.1038/s41380-023-02223-8.

78. Poulin, J.F., Gaertner, Z., Moreno-Ramos, O.A., and Awatramani, R. (2020). Classification of midbrain dopamine neurons using single-cell gene expression profiling approaches. Trends Neurosci. *43*, 155–169. https://doi.org/10.1016/j.tins.2020.01.004.

79. Liu, Z., Li, X., Zhang, J.T., Cai, Y.J., Cheng, T.L., Cheng, C., Wang, Y., Zhang, C.C., Nie, Y.H., Chen, Z.F., et al. (2016). Autism-like behaviours and germline transmission in transgenic monkeys overexpressing MeCP2. Nature *530*, 98–102. https://doi.org/10.1038/nature16533.

80. Golden, C.E.M., Breen, M.S., Koro, L., Sonar, S., Niblo, K., Browne, A., Burlant, N., Di Marino, D., De Rubeis, S., Baxter, M.G., et al. (2019). Deletion of the KH1 domain of Fmr1 leads to transcriptional alterations and attentional deficits in rats. Cereb. Cortex *29*, 2228–2244. https://doi.org/10.1093/cercor/bhz029.

81. Lacey, M.G., Mercuri, N.B., and North, R.A. (1989). Two cell types in rat substantia nigra zona compacta distinguished by membrane properties and the actions of dopamine and opioids. J. Neurosci. *9*, 1233–1241. https://doi.org/10.1523/JNEUROSCI.09-04-01233.1989.

82. Tian, C., Wang, K., Ke, W., Guo, H., and Shu, Y. (2014). Molecular identity of axonal sodium channels in human cortical pyramidal cells. Front. Cell. Neurosci. *8*, 297. https://doi.org/10.3389/fncel.2014.00297.

83. Kramer, P.F., Twedell, E.L., Shin, J.H., Zhang, R., and Khaliq, Z.M. (2020). Axonal mechanisms mediating γ-aminobutyric acid receptor type A (GABA-A) inhibition of striatal dopamine release. eLife *9*, e55729. https://doi.org/10.7554/eLife.55729.

84. Rein, B., Ma, K., and Yan, Z. (2020). A standardized social preference protocol for measuring social deficits in mouse models of autism. Nat. Protoc. *15*, 3464–3477. https://doi.org/10.1038/s41596-020-0382-9.

85. Simpson, E.H., Akam, T., Patriarchi, T., Blanco-Pozo, M., Burgeno, L.M., Mohebi, A., Cragg, S.J., and Walton, M.E. (2024). Lights, fiber, action! A primer on in vivo fiber photometry. Neuron *112*, 718–739. https://doi.org/10.1016/j.neuron.2023.11.016.

86. Meng, C., Zhou, J., Papaneri, A., Peddada, T., Xu, K., and Cui, G. (2018). Spectrally resolved fiber photometry for multi-component analysis of brain circuits. Neuron *98*, 707–717.e4. https://doi.org/10.1016/j.neuron.2018.04.012.

87. Deng, F., Wan, J., Li, G., Dong, H., Xia, X., Wang, Y., Li, X., Zhuang, C., Zheng, Y., Liu, L., et al. (2024). Improved green and red GRAB sensors for monitoring spatiotemporal serotonin release in vivo. Nat. Methods *21*, 692–702. https://doi.org/10.1038/s41592-024-02188-8.

Please cite this article in press as: Li et al., Selective loss of *Scn2a* in ventral tegmental area dopaminergic neurons leads to dopamine system hypofunction and autistic-like behaviors, Neuron (2025), https://doi.org/10.1016/j.neuron.2025.06.003

STAR★METHODS

KEY RESOURCES TABLE

REAGENT or RESOURCE	SOURCE	IDENTIFIER
Antibodies		
Rabbit anti-TH	Millipore	Cat#AB152; RRID:AB_390204
Mouse anti-Nav1.2	NeuroMab	Cat#73-024; RRID:AB_10673401
Rabbit ant-Nav1.6	Alomone Labs	Cat#ASC-009; RRID:AB_2040202
Goat anti-Ankyrin G	Santa Cruz Biotechnology	Cat#sc-31778; RRID:AB_2289736
Mouse anti-GFP	Thermo Fisher Scientific	Cat#MA5-15349; RRID:AB_10987186
Donkey anti-rabbit Alexa Fluor 405	Abcam	Cat#ab175651; RRID:AB_2923541
Donkey anti-rabbit Alexa Fluor 488	Thermo Fisher Scientific	Cat#A-21206; RRID:AB_2535792
Donkey anti-mouse Alexa Fluor 555	Thermo Fisher Scientific	Cat#A-31570; RRID:AB_2536180
Donkey anti-rabbit Alexa Fluro 555	Thermo Fisher Scientific	Cat#A-31572; RRID:AB_162543
Donkey anti-mouse Alexa Fluro 647	Jackson ImmunoResearch Labs	Cat#715-605-151; RRID:AB_2340863
Donkey anti-goat Alexa Fluor 647	Thermo Fisher Scientific	Cat#A-21447; RRID:AB_2535864
Goat anti-mouse Alexa Fluor 488	Thermo Fisher Scientific	Cat#A32723; RRID:AB_2633275
Bacterial and Virus Strains		
AAV2/9-(H1-gRNA)×3-CAG-EGFP	Taitool Bioscience, Shanghai	Cat#AAV2/9-WY2914
AAV2/9-(H1-gRNA-scamble)×3-CAG-EGFP	Taitool Bioscience, Shanghai	Cat#AAV2/9-WY3487
AAV2/9-CAG-EGFP	Taitool Bioscience, Shanghai	Cat#S0582-9
AAV2/9-TH-Cre-EGFP	OBiO Technology, Shanghai	Cat#H17836
AAV2/9-TH-EGFP	OBiO Technology, Shanghai	Cat#H23714
AAV9-hSyn-rDA3m	Brain Case, Shenzhen	Cat#BC-0785
AAV2/9-EF1α-DIO-ChR2(H134R)-EYFP	BrainVTA, Wuhan	Cat#PT-0001
AAV2/9-TH-NLS-Cre	BrainVTA, Wuhan	Cat#PT-0179
Chemicals, Peptides, and Recombinant Proteins		
Streptavidin, Alexa Fluor 488 conjugate	Thermo Fisher Scientific	Cat#S11223
Streptavidin, Alexa Fluor 647 conjugate	Thermo Fisher Scientific	Cat#S21374
Levodopa	Sigma-Aldrich	Cat#D9628; CAS:59-92-7
Benserazide	Sigma-Aldrich	Cat#B7283; CAS:14919-77-8
Kynurenic acid	Sigma-Aldrich	Cat#K3375; CAS:492-27-3
Carbachol	Abcam	Cat#ab141354; CAS:51-83-2
SCH 39166	Tocris Bioscience	Cat#2299; CAS:1227675-51-5
SCH 23390	Tocris Bioscience	Cat#0925; CAS:125941-87-9
Tetrodotoxin	Tocris Bioscience	Cat#1078; CAS:4368-28-9
Picotocin	Tocris Bioscience	Cat#1128; CAS:124-87-8
RNAscope Probe-Mm-Scn1a-C2	Advanced Cell Diagnostics	Cat#556181-C2
RNAscope Probe-Mm-Scn2a	Advanced Cell Diagnostics	Cat#423641
RNAscope Probe-Mm-Scn3a-C2	Advanced Cell Diagnostics	Cat#502641-C2
RNAscope Probe-Mm-Scn5a	Advanced Cell Diagnostics	Cat#429881
RNAscope Probe-Mm-Scn8a-C2	Advanced Cell Diagnostics	Cat#434191-C2
RNAscope Probe-Mm-Scn9a-C3	Advanced Cell Diagnostics	Cat#313341-C3
RNAscope Probe-Mm-Scn10a-C2	Advanced Cell Diagnostics	Cat#426011-C2
RNAscope Probe-Mm-Scn11a	Advanced Cell Diagnostics	Cat#403531

(*Continued on next page*)

Please cite this article in press as: Li et al., Selective loss of *Scn2a* in ventral tegmental area dopaminergic neurons leads to dopamine system hypofunction and autistic-like behaviors, Neuron (2025), https://doi.org/10.1016/j.neuron.2025.06.003

Continued

REAGENT or RESOURCE	SOURCE	IDENTIFIER
Experimental Models: Organisms/Strains		
Mouse: Dat-Cre	Jackson Laboratory	Strain#006660; RRID:IMSR_JAX:006660
Mouse: Cas9 floxed	GemPharmatech	Strain#T002249; RRID:IMSR_GPT:T002249
Mouse: *Scn2a* floxed	Cyagen	Strain#S-CKO-00900
Mouse: *Scn2a*$^{+/-}$	Cyagen	Strain#S-KO-00789
Mouse: *Scn8a*-KO	Jackson Laboratory	Strain#003798; RRID:IMSR_JAX:003798
Mouse: Thy1-Cre	Jackson Laboratory	Strain#006143; RRID:IMSR_JAX:006143
Mouse: C57BL/6J	GemPharmatech	Strain#N000295
Oligonucleotides		
Scn2a #1 Fwd Primer: GCTAAGAG ACCCAAACAGGAACGC	This paper	N/A
Scn2a #1 Rev Primer: GCAGCCCG ATGAGAGCAAAGACAC	This paper	N/A
Scn2a #2 Fwd Primer: GCAAGGAC GAAGACGACGAAAATG	This paper	N/A
Scn2a #2 Rev Primer: TTCTTCACC GACTGGATCAGGGCC	This paper	N/A
Scn2a #3 Fwd Primer: AGAGATG GTGTCAGAGCCCC	This paper	N/A
Scn2a #3 Rev Primer: AGTTCGAA GAGCTGAAACATTGCC	This paper	N/A
Software and Algorithms		
Spike2 Software 10	Cambridge Electronic Design	http://ced.co.uk/downloads/latestsoftware; RRID:SCR_000903
pCLAMP sofrware10	Molecular Devices	https://www.moleculardevices.com/; RRID: SCR_011323
ANY-maze	Stoelting	https://www.any-maze.com; RRID:SCR_014289
MATLAB R2017b and R2022a	MATHWORKS	https://www.mathworks.com/; RRID: SCR_001622
ImageJ	NIH	https://imagej.net/Welcome; RRID: SCR_003070
ICE	Synthego	https://ice.synthego.com
Prism 9 and 10	GraphPad Software	https://www.graphpad.com/scientific-software/prism/; RRID: SCR_002798
Adobe Illustrator 2024	Adobe	https://www.adobe.com/; RRID: SCR_010279
Original code	This paper	https://doi.org/10.5281/zenodo.15597751

EXPERIMENTAL MODEL AND STUDY PARTICIPANT DETAILS

All experiments were performed on mice in accordance with protocols approved by the Animal Care and Use Committee at Fudan University. Transgenic mice of *Dat*^{Cre} mice (JAX, 006660), *Scn8a*^{KO} mice (JAX, 003798) and *Thy1*^{Cre} mice (JAX, 006143) were obtained from the Jackson Laboratories. CAG-LSL-Cas9-tdTomato mice (T002249) and wild-type (WT) C57BL/6J mice (N000295) were obtained from GemPharmatech. *Scn2a* floxed mice were generated by inserting LoxP sites into the intron 3 and the intron 6 to cause deletion of exon 4-6 in the presence of Cre-recombinase (Figure S3A, Cyagen). *Scn2a*$^{+/-}$ mice were generated by deletion of exon 4-6 of *Scn2a* gene (Cyagen, S-KO-00789). All mice, except for *Scn8a*^{KO} (C3HeB/FeJ background) and *Thy1*^{Cre} (FV B/N background), were on a C57BL/6J background. *Dat*^{Cre} and *Thy1*^{Cre} mice were crossed with *Cas9*^{fl} mice to generate offspring expressing both Cas9 and tdTomato in *Dat*$^{+}$ and *Thy1*$^{+}$ neurons, respectively. Mice were group-housed under a 12-hr light/dark cycle with *ad libitum* access to food and water in the Animal Facility of the Department of Laboratory Animal Science, Fudan University. All experiments were conducted during the light cycle (8 a.m. to 8 p.m.). Both male and female mice (during the diestrus phase) were used in experiments, except for the fiber photometry, behavior tests, and slice recordings from *Scn2a*$^{+/-}$ mice where only male mice were utilized.

Fluorescent *in situ* hybridization was performed on WT mice aged 6-8 weeks. *Dat*^{Cre}::*Cas9*^{fl} mice received viral injections at 4-5 weeks of age, and electrophysiological recordings were conducted at postnatal day (P) 62-91. *Thy1*^{Cre}::*Cas9*^{fl} mice received viral injections at P40-43 and underwent slice recordings at P61-63. *Scn2a* floxed mice received viral injections at 4-7 weeks of age, and slice imaging was performed at 8-12 weeks of age. We performed slice recordings from *Scn8a*^{KO} mice and their WT littermates at

P17-23. For immunofluorescence staining at different developmental stages, we obtained brain sections from neonatal (P7–9), juvenile (P17–25), and adult (P61–152) mice. Behavior tests were performed on mice aged 2-3 months. Fiber photometry was conducted in *Scn2a* floxed mice and Dat^{Cre}::$Cas9^{fl}$ mice at 8-10 weeks of age, and $Scn2a^{+/-}$ mice at 13 weeks of age.

METHOD DETAILS

Fluorescent *in situ* hybridization

Wild-type mice at 6-8 weeks old were anesthetized with sodium pentobarbital (100 mg·kg^{-1}, i.p.). Mice received transcardiac perfusion with 0.01 M phosphate-buffered saline (PBS, pH 7.4), and then with ice-cold 4% paraformaldehyde (PFA, in 0.1 M phosphate buffer, PB). The brain was dissected out and post-fixed in 4% PFA for 24 hr. Then the brain was immersed in 15% sucrose at 4°C until sunk to the bottom of the container and repeated with 30% sucrose. 10-μm-thick sections containing the midbrain were prepared using a cryostat (CM1950, Leica), and continuous sections were mounted on separate glass slides. For labelling the eight potential Na_V subtypes in DANs, we used RNAscope Multiplex Fluorescent Reagent Kit v2 (ACD Bio, #323100) combined with RNA-Protein Co-Detection Ancillary kit (ACD Bio, #323180) to protect antigenic epitopes during the procedure of RNAscope.

We treated the sections with protease III for 25 min at 40 °C in the humid HybEZ Oven (#321721). Each slide was hybridized with a mixture of two probes for different channel subtypes. The following probes were used: *Scn1a* (#556181-C2), *Scn2a* (#423641), *Scn3a* (#502641-C2), *Scn5a* (#429881), *Scn8a* (#434191-C2), *Scn9a* (#313341-C3), *Scn10a* (#426011-C2) and *Scn11a* (#403531). Control probes of 3-plex positive (#320881) and 3-plex negative (#320871) were applied to examine the quality of RNAscope experiments. To avoid any effect of the wavelength of emitting light on the sharpness of the particles, probes conjugated with Opal 570 or Opal 690 were counterbalanced in different experiments. The sections were incubated with rabbit anti-TH antibody (1:200, Chemicon, AB152) overnight at 4 °C, followed by incubation with Alexa Fluor 488-conjugated donkey anti-rabbit (1:1000, invitrogen, A21206) diluted in Co-Detection Antibody Diluent for 2 hr at room temperature (RT). After washed in PBS, slides underwent DAPI staining for 30 s at RT, and were mounted with fluoromount-G (Electron Microscopy Sciences, Cat. No.17984-25). In the experiment including EGFP expression in the tissue, mouse anti-GFP antibody (1:200, Invitrogen, MA5-15349) was applied to reserve its signals. Alexa Fluor 555 conjugated donkey anti-mouse (1:1000, A-31570) and Alexa Fluor 488-conjugated goat anti-mouse (1:1000, A32723) were used as the secondary antibodies.

We took z-stack images with a single-plane thickness of 0.5 μm using a 20× air objective or a 60× oil-immersion objective on a confocal microscope (Nikon C2). We used Fiji software (https://imagej.net/downloads) to analyze mRNA copy number in each neuron. The soma sectional area of a TH^+ cell (S_{cell}) and the area of its mRNA signals (S_{mRNA}) were selected and segmented by adjusting the threshold of fluorescent signals. Considering that the mRNA signals may cluster together, making it difficult to distinguish individual particles, we first obtained the average area (or pixel numbers) of each mRNA particle ($\overline{S}$) by analyzing those particles that separate from each other, then we divided the total mRNA signal area (S_{mRNA}) by the $\overline{S}$ to obtain the number of mRNA particles per cell ($S_{mRNA}/\overline{S}$).

Stereotaxic surgeries

Mice were anesthetized initially with 3%-4% isoflurane in an induction chamber and maintained anesthesia with 1.5%-2% isoflurane on a stereotaxic apparatus. After trimming the hair and exposing the skull, we cleaned the skull with 3% hydrogen peroxide and drilled small holes above the target brain regions (coordinates in mm relative to bregma, VTA: AP -3.20, ML ±0.45, DV -4.30; mPFC, AP +1.94, ML ±0.34, DV -2.00; SNc: AP -3.00, ML ±1.40, DV -4.10). Viruses were infused at a rate of 50-80 nl/min through a hydraulic microinjector (SMO-10C, Narishige). After injection, the needle was left in place for 10 min and then slowly retracted to avoid leakage of the injected solution. Three different *gRNA*s (*gRNA1*, TGAAGGGAGTTAAAATGTAC; *gRNA2*, CATGGTCA TAAATACACAGT; *gRNA3*, TAGAAGATTTCACATTTCTA) targeting *Scn2a* (GenBank: NM_001099298.2) were cloned to make $AAV_{2/9}$-(H1-gRNA)×3-CAG-EGFP (*gRNA*, or AAV-*gRNA*-EGFP for short, 1.74×10^{13} vg/ml, Taitool). In addition, viruses with scrambled *gRNA*s (*scram*) targeting the same gene sites (*scram1*, TTGTAAAGAGAGAAGTTGCA; *scram2*, TAAGATATTGTAATTTA CCC; *scram3*, ACACTCGTCAGTTATAAAGA. 1.10×10^{13} vg/ml, Taitool) or with *gRNA* omitted (denoted as *ΔgRNA*, 1.86×10^{13} vg/ml, Taitool) were made as controls. Dat^{Cre}::$Cas9^{fl}$ mice at 4-5 weeks old received injection of the same virus to VTA at a volume of 150 nl/site or SNc at a volume of 50 nl/site. $Thy1^{Cre}$::$Cas9^{fl}$ mice at P40-43 were infected with the virus containing *gRNA*s to the left mPFC and that of *ΔgRNA* to the right hemisphere at a volume of 200 nl/site. Mice with similar surgeries were housed together and allowed to recover for at least 4 weeks unless otherwise stated. All viruses were stored at -80 °C until use.

Electrophysiological recording

For whole-cell recording at the soma, coronal brain slices containing midbrain (200 μm in thickness) or mPFC (300 μm) were obtained from adult Dat^{Cre}::$Cas9^{fl}$ (P62-91) or $Thy1^{Cre}$::$Cas9^{fl}$ mice (P61-63), respectively. After deep anesthesia with sodium pentobarbital (100 mg·kg^{-1}, i.p.), animals were transcardially perfused with 10-15 ml ice-cold slicing solution that was pre-equilibrated with carbogen (95% O_2 and 5% CO_2) and containing (in mM) NaCl 75, sucrose 75, KCl 2.5, $NaH_2PO_4{\cdot}2H_2O$ 1, $NaHCO_3$ 26.2, dextrose 12, $MgSO_4{\cdot}7H_2O$ 7.5, myo-inositol 1, sodium pyruvate 3 and ascorbic acid 1,[44] followed by decapitation and immersion of the heads into the slicing solution. The brain tissue was then exposed by removing the skull and carefully dissected out. Brain slices were sectioned using a vibratome (Leica, VT1200s) with a speed of 0.10 mm/s and a vibration amplitude of 0.80 mm. Midbrain slices were cut thinner than those of mPFC slices to facilitate visualization of DANs with differential interference contrast (DIC) imaging.

The slices were incubated in oxygenated artificial cerebrospinal fluid (ACSF) containing (in mM): NaCl 126, KCl 2.5, $NaH_2PO_4{\cdot}H_2O$ 1.25, $NaHCO_3$ 26, dextrose 25, $MgSO_4$ 2 and $CaCl_2$ 2 (315 mOsm, pH 7.4) at ~34.5 °C for 40-50 min, and then placed at RT for at least 30 min before recording. Homozygous *Scn8a*^{KO} mice and their WT littermates were used for experiments at P17-23 because the KO mice would die around postnatal 3 weeks. Juvenile mice were decapitated after anesthesia without transcardiac perfusion and brain slices were cut in sucrose slicing solution containing (in mM): sucrose 213, dextrose 10, KCl 2.5, $NaH_2PO_4{\cdot}H_2O$ 1.25, $NaHCO_3$ 26, $MgSO_4$ 2, $CaCl_2$ 2.

We performed whole-cell patch clamp recordings from slices perfused with oxygenated ACSF at ~34 °C to examine neuronal excitability and membrane properties. Midbrain or mPFC neurons were visualized under an infrared DIC microscope (BX51WI, Olympus) with a 40× water immersion objective. Real-time DIC images were captured by a CCD camera and displayed on a monitor. Fluorescent proteins or other fluorophores were excited by LED beams with wavelengths of 530-550 nm or 460-490 nm. We performed recordings from *Dat*$^+$ cells or *Thy1*$^+$ cells double positive to tdTomato and EGFP, reflecting the expression of Cas9 and the infection of viruses. In some experiments, recordings were made from tdTomato-only cells. In experiments recording from cells without fluorescent tags, we distinguished DANs from non-dopaminergic neurons by two distinct electrophysiological characteristics: 1) the initial depolarization ramp (due to the rapid activation and inactivation of A-type K^+ currents) in response to 500-ms step current injections; 2) the broad AP waveforms (> 0.5 ms).[37,81] 69.1% *Th*$^+$ neurons (n = 470) exhibited electrophysiological characteristics of DANs. Membrane potential or current signals were amplified by a MultiClamp 700B amplifier (Molecular devices), acquired by Micro1401-3 (Cambridge electronic design, CED) together with Spike2 software (Version 8, CED). The signals were recorded at 25 or 50 kHz and filtered with Bessel filter at 10 kHz. The patch pipettes had an impedance of 4-7 MΩ when filled with normal intracellular solution containing (in mM): Kgluconate 140, KCl 3, $MgCl_2$ 2, HEPES 10, EGTA 0.2, Na_2ATP 2 and biocytin 0.2% (280-290 mOsm, pH 7.2-7.3). Cells with series resistances less than 25 MΩ and <20% change during recording were included for data analysis.

In midbrain DANs, the spontaneous firing frequency is analyzed as the average number of discharges within 30 s after reaching a stable recording. To examine the AP waveforms and related parameters, we evoked APs with 500-ms step current injections at rheobase, i.e., threshold current that can evoke APs with a probability of 0.5. The voltage threshold of AP is defined as the membrane potential at which the depolarizing rate reaches 20 V/s. The AP amplitude is the membrane potential difference between the threshold and the peak. The AP half-width is calculated as the duration at half amplitude. The peak d*V*/d*t* is the maximum slope in the AP depolarizing phase, while the peak repolarization d*V*/d*t* is the minimum slope in the repolarizing phase. Membrane potential changes induced by a negative current pulse of -60 pA are used to measure the input resistance. In neocortical PCs, we chose to analyze the first AP in a train with a firing frequency at 20 Hz. The resting membrane potential of PCs is measured when there is no holding current.

To investigate the effect of *Scn2a* deletion on AP propagation in DANs, we performed dual soma and bleb recordings in current-clamp mode. Alexa Fluor 555 was added into the pipette for somatic recording to label all the neurites including the axonal compartments. After identification of the corresponding axonal bleb, another patch pipette with an impedance of 8-10 MΩ (without adding fluorescence dyes) was used to form whole-cell recording from the bleb. Current pulse stimulations at the soma or the axon bleb were used to generate APs and examine their orthodromic conduction and backpropagation, respectively. We performed *post hoc* staining with streptavidin conjugated Alexa Fluor 647 and confocal microscope imaging to obtain the morphology of the recorded cells.

To examine the responses of DANs to opto-stimulation, we carried out whole-cell recording in current clamp mode from ChR2-expressing VTA DANs in control mice and delivered 473-nm light pulses (1 ms in duration). No holding current was applied to the recorded cell. We added 1.5 mM kynurenic acid (Kyn, Sigma) and 50 μM picrotoxin (PTX, Tocris) to the bath solution to block fast glutamatergic and GABAergic synaptic transmission, respectively.

In experiments recording Na^+ currents, we conducted patch clamp recordings from nucleated patches and axonal blebs from VTA DANs. To isolate the Na^+ currents, we added $CdCl_2$ (200 μM, Sigma), 4-AP (3 mM, Sigma) and TEA (20 mM, Sigma) to the ACSF to block voltage-gated Ca^{2+} channels and K^+ channels, and used a Cs-based internal solution containing (in mM): CsCl 125, NaCl 10, $MgCl_2$ 2, $CaCl_2$ 0.5, Na_2ATP 2, Na_3GTP 0.5, HEPES 10, EGTA 10, TEA 2 and biocytin 0.2%. Isolated axonal blebs were obtained by sweeping a patch pipette just underneath the blebs. Patch pipettes for recording had an impedance of 4-6 MΩ for nucleated patches, 8-10 MΩ for blebs of axon trunks, and 11-13 MΩ for blebs of axon terminal branches. Na^+ currents were evoked by a series of voltage steps (50 ms in duration, from -70 to +30 mV, ΔV = 10 mV for soma; from -70 to +10 mV, ΔV = 5 mV for isolated axonal blebs) from a 50-ms prepulse at -100 mV. The liquid junction potential (approximately 15.8 mV) was not corrected for all the data shown in the text and figures.

Immunofluorescence staining

For brain tissue preparation for $Na_V1.2$ immunostaining, we perfused the animals with a weak fixative (0.5% PFA and 0.5% sucrose in 0.1 M PB) as previously reported.[16,17,82] After anesthesia with sodium pentobarbital (100 mg·kg^{-1}, i.p.), we transcardially perfused them with 0.9% (wt/vol) saline to wash out the blood, followed by an ice-cold weak fixative (~15 ml, 2-min perfusion). The brains were dissected out and postfixed in similar fixative for 2 hr, and then transferred to 30% sucrose (in PBS, 4 °C) for at least 24 hr. For experiments examining $Na_V1.2$ distribution and gene-editing efficacy of AAV-*gRNA*s, we prepared acute slices just like those for electrophysiological recordings because tissues without PFA perfusion of the whole animal showed more robust immunosignals.[82] In brief, we cut acute slices (300 μm in thickness) and fixed them in the weak fixative for 45 min. Then the slices were transferred into 30% sucrose for 1 hr. They were cut into 20-μm-thick sections in the cryostat at -20 °C. To examine the distribution pattern of $Na_V1.2$ in VTA DANs or mPFC PCs, we rinsed the sections in PBS, and treated them with 0.5% TritonX-100 in PBS (PBS-T) for 30 min at RT. After incubation in a blocking solution of 5% bovine serum albumin (BSA, in 0.1% PBS-T) for 1 hr, the sections

were treated with primary antibodies (diluted with 0.1% PBS-T) including mouse anti-$Na_V1.2$ (1:200; 73-024, NeuroMab), rabbit anti-TH or rabbit anti-$Na_V1.6$ (1:1000; ASC-009, Alomone Labs), and goat anti-AnkG (1:500; sc-31778, Santa cruz) for 18-24 hr at 4 °C. The sections were then incubated with the secondary antibodies (1:1000; Invitrogen) including Alexa Fluor 555 conjugated donkey anti-mouse, Alexa Fluor 488 conjugated donkey anti-rabbit and Alexa Fluor 647 conjugated donkey anti-goat (A-21447) for 2 hr at RT. Sections were completely washed in PBS every time after antibody incubation. In our experiments, the injection of AAV-*gRNA*s into the mPFC and VTA dramatically diminished the immunosignals of $Na_V1.2$, confirming a high specificity of the $Na_V1.2$ antibody (Figures 1E, S2A, and S2C).

For staining of the biocytin-loaded cells together with TH immunostaining after electrophysiological recordings, the acute brain slices were fixed in 4% PFA overnight. After washed in PBS, the free-floating slices were treated with 0.5% PBS-T for 1-2 hr, and then incubated in 5% BSA for 2 hr. The slices were incubated in streptavidin conjugated by either Alexa Fluor 647 (1:1000; S21374, Thermo Fisher Scientific) or Alexa Fluor 488 (1:1000; S11223), and the primary antibody of rabbit anti-TH in 0.1% PBS-T at 4 °C overnight. After washed in PBS, the slices were treated with a secondary antibody of either Alexa Fluor 405 conjugated donkey anti-rabbit (1:500; ab175651, Abcam) or Alexa Fluor 555 conjugated donkey anti-rabbit (1:1000; A31572, Invitrogen), and DAPI in 0.1% PBS-T for ~6 hr at RT. The slices were then mounted on slides with fluoromount-G and stored at -20 °C.

Images were captured by a laser scanning confocal microscope (Nikon A1 plus) with a set of objectives including 10× (NA 0.7) or 20× (NA 0.8) air objective, 25× (NA 1.1) water-immersion objective, and 60× (NA 1.4) oil-immersion objective or a slide scanner (Olympus SLIDEVIEW VS200) with 10× objective (NA 0.4). The voxel interval of z-step was set to 0.5 or 1 μm. We employed ImageJ software to adjust brightness and contrast of images, obtained appropriate projection of z stacks or merged images of different signal channels, and virus efficiency analysis. To assess the efficiency of the *Th* promotor, we injected viruses (AAV-TH-Cre-EGFP, 1.35×10^{13} vg/ml, or AAV-TH-EGFP, 1.72×10^{13} vg/ml, OBiO) into the VTA of mice. Four weeks after the injection, we obtained three VTA sections (~200 μm apart) from each mouse and stained them with TH antibodies to identify DANs. We then calculated the percentage of TH/EGFP positive cells in all TH-immunoreactive cells or $EGFP^+$ cells. To assess the infection efficiency of AAV-*gRNA*-EGFP, we manually delineated the boundaries of the VTA and SNc based on TH^+ area and the brain atlas. The proportion of infected area was calculated as the ratio of $EGFP^+$ area to the total area of the VTA or SNc. The midbrain regions ranging from -2.79 to -3.87 mm (with an interval of 0.12 mm) relative to the bregma were included for this measurement.

Single-cell RNA-sequencing of gRNA *targeted locus*

Before electrophysiological recordings, the equipment was wiped with RNase Zap and 75% ethanol to prevent RNase contamination. Recombinant RNase Inhibitor (Takara, 2313A) was added into the intracellular solution to prevent mRNA degradation. Positive pressure was applied to the pipette before entering the bath solution. Whole-cell recording was performed on tdTomoto/EGFP positive cells (i.e., Dat^+ cells expressing *gRNA* or *ΔgRNA*) in midbrain slices of Dat^{Cre}::$Cas9^{fl}$ mice that received injections of viruses (AAV-*ΔgRNA*-EGFP or AAV-*gRNA*-EGFP) in VTA. The cell contents were aspirated into the pipette, and collected by forming nucleated patch (containing the cell nucleus and cytosol), then transferred into lysis buffer. The sequence of the *gRNA*-targeted locus was amplified using Smart-seq2 and nested PCR (first round primers sequences are: forward primer 5'-gctaagagacccaaacaggaacgc and reverse primer 5'-gcagcccgatgagagcaaagacac; second round primers sequences are: forward primer 5'-gcaaggacgaagacgacgaaaatg and reverse primer 5'-ttcttcaccgactggatcagggcc; third round primers sequences are: forward primer 5'-agagatggtgtcagagcccc and reverse primer 5'-agttcgaagagctgaaacattgcc), followed by Sanger sequencing. The frequency of indel and knockout efficiency were analyzed by ICE software (https://ice.synthego.com).

Imaging dopamine release in brain slices

$Scn2a^{fl/fl}$ mice of 4 weeks old received bilateral injections of the abovementioned viruses using the *Th* as a promoter in VTA (150 nl per site), as well as injections of the AAV_9-hSyn-rDA3m (AAV-hSyn-rDA3m for short, 1.03×10^{13} vg/ml, BrainCase) to the NAc (200 nl per site, coordinates relative to bregma in mm: AP +1.50, ML ±1.09, DV -4.60). Using similar protocols for acute slice preparation, we obtained coronal slices (300 μm in thickness) containing the NAc 4-5 weeks after the virus injection. The slice imaging was conducted in a recording chamber perfused with oxygenated ACSF (~34 °C). A concentric bipolar electrode (SKU30205, Lot#300078, FHC) was placed at the NAc core with intense $EGFP^+$ (Th^+) fibers and rDA3m expression. Single or trains of electric shocks (0.1 ms in pulse duration) were delivered to the tissue to evoke changes of rDA3m fluorescence that reflect dopamine levels. We also puffed 100 μM carbachol (Abcam) or 500 μM levodopa (Sigma) to the NAc core with glass pipettes (similar to those used for somatic recording) by a pressure ejection (~10 psi, 2 s per pulse; Picospritzer III, PARKER HANNIFIN). The glass pipettes were also filled with 100 μM Alexa Fluor 488, which allowed visualization of the puff region. The rDA3m was excited by a 580-nm light beam, and the fluorescence was collected with a 40× water-immersion objective and captured using an Iris 9 sCMOS camera (Teledyne Photometrics). The exposure time was set to 100 ms/frame, and images (740 × 740 pixels/frame) were acquired at 10 frames/s. The pixel size was 0.425 × 0.425 μm^2.

To optogenetically activate dopaminergic axons in the NAc, we bilaterally injected a mixture of $AAV_{2/9}$-TH-NLS-Cre (AAV-TH-Cre for short, 1.19×10^{13} vg/ml, Brainvta) and $AAV_{2/9}$-EF1α-DIO-ChR2(H134R)-EYFP (AAV-DIO-ChR2-EYFP for short, 5.18×10^{12} vg/ml, Brainvta) into the VTA of C57BL/6J WT mice or $Scn2a^{fl/fl}$ mice (5-7 weeks old), with a total volume of 150 nl/site at a 1:2 volume ratio. Additionally, the AAV-hSyn-rDA3m was injected into the NAc to allow expression of rDA3m by local neurons. Five weeks after the virus injection, dopamine sensor imaging was conducted on 300-μm-thick coronal slices containing the NAc. We added 1.5 mM Kyn and 50 μM PTX to the bath solution as mentioned before. The rDA3m signals were acquired at 10 frames/s with a 50 ms/frame

exposure. To activate the ChR2-expressing Th^+ axon terminals and prevent light artifacts, we used a 470-nm fiber laser (PSU, CNI) to deliver a light pulse (1 ms in pulse duration) with a 30-ms delay after the cessation of each 50-ms camera exposure. The laser and camera were synchronized using a Master-8 stimulator (AMPI). The power of the laser was measured when it gave constant output. In these experiments, bath application of tetrodotoxin (TTX, 1 μM) suppressed most of the light-evoked dopamine release, but we still observed a small residual signal that could be further abolished by the removal of extracellular Ca^{2+} (Figures S11F–S11I). The TTX-resistant release may be attributed to the presence of PTX, which could eliminate $GABA_A$ receptor-mediated shunting inhibition of axons and thereby enhance light-induced depolarization.[83]

The ROI for analysis was the entire field imaged with a 40× objective lens (314 μm × 314 μm), excluding the region covered by the electrode tip (i.e., the completely black region). We utilized custom-written codes to analyze and extract rDA3m fluorescence signal. Data analysis includes noise reduction, up-sampling, baseline correction, pixel screening, and fluorescence change calculation. Initially, the DeepCAD-RT algorithm was applied to batch reduce noise in images, aiming to minimize scattering noise from the optical imaging system (using default settings of the deepcad_model, patch_xy = 150, patch_t = 150, overlap_factor = 0.60). Subsequently, data points were up-sampled 30-fold from the original 10 to 300 data points/s using the fit (with a smoothing spline model) and feval functions in MATLAB, to smooth the fluorescence signal curve. Accounting for variable photobleaching rates across different field of view locations, an adaptive linear regression was employed to individually fit and calculate the signal decay rate for each pixel from 0.5 to 5 seconds after the imaging onset. This decay rate, designated as the standard rate of photobleaching (v_0), was then used as the slope for generating a baseline with a 20-s decay period. To quantify the area with fluorescence changes, pixels exhibiting $\Delta F/F_0$ greater than 5% throughout the imaging duration were identified as part of a responsive region (Figures 4G and S11J). The average fluorescence change within this region was calculated over the 20-s imaging period.

Behavior tests

We performed the behavior tests on male mice (2-3 months old) group-housed according to their experimental groups. Mice were carefully habituated to handling for at least three days prior to the experiments to minimize stress. The mice were allowed to habituate in the behavior test room for more than 1 hr before the tests. All test apparatuses were cleaned with 75% ethanol and allowed to air dry completely between trials. Animal behaviors were quantified using ANY-maze software or *BehaviorAtlas*.[48]

Open field test

Mice are introduced into an open box (dimensions: 35 cm × 35 cm × 35 cm) for a 10-min period, and their locomotion is quantified based on the total distance traveled in the field. Repetitive circular locomotion is defined as a mouse ambulating in the same direction with at least two laps within 20 s. The number of circular locomotion events was manually counted by two experimenters who were blinded to the experimental conditions, and the average value was taken for final quantification.

Analysis of spontaneous behavior

Three-dimensional behavior of the mouse within a 30-min period in the transparent open-field box was recorded by four lateral cameras and reconstructed offline.[48] The motion of the mouse was tracked and analyzed using *BehaviorAtlas* with 16 body points (including nose, ears, neck, back, claws, limps, as well as root, middle and tip of the tail). Forty behavior clusters were identified and then manually categorized into sniffing, grooming, rearing, jumping, turning, or ambulating.

Elevated plus maze test

Anxiety levels of the test mouse was assessed using an elevated plus maze (EPM, length: 63 cm for each arm, height: 50 cm) with two open arms and two closed arms. The test was conducted under a light intensity of 130 lux. The mouse was introduced at the cross center, facing one of the closed arms, and allowed to freely explore the maze for 6 min. Time spent in open (t_{open}) and closed (t_{closed}) arms was recorded, and the time ratio for each was calculated relative to the total test duration (t_{total}), i.e., (t_{open} or t_{closed})/t_{total}. The open arms exploration index was calculated as the ratio of time spent in open arms to the total time in arms, i.e., $t_{open}/(t_{open} + t_{closed})$.

Resident-intruder test

The test mouse experienced social isolation for 4 hr in its home cage before the test. A junior novel intruder (6 weeks old, male conspecific) was introduced to the home cage of the test mouse and allowed free social interaction for 10 min. Spontaneous behaviors were videotaped with a camera above the cage. Proactive social interactions were manually timed, including closely chasing, body or anogenital sniffing, and direct contacts initiated by the test mice. The total duration of the proactive social interactions was used for comparison between different mouse groups.

Social preference and social novelty preference tests

The social preference and the social novelty preference tests were carried out as described previously,[84] but with the clapboards removed to minimize the impact of circular locomotion on social exploration, otherwise the *gRNA* mice might be confined in a single compartment. In this modified chamber, the test mouse was able to freely explore the social targets without shuttling between compartments. There were three 10-min test sessions in the social behavior tests, including the pre-test, the social preference test, and the social novelty preference test. The tests were conducted in a transparent plexiglass apparatus (dimensions: 100 cm × 45 cm × 45 cm) which is large enough for the test mouse to explore. Before the experiment, the test mouse was placed in the center and allowed to explore for 10 min twice a day. Two wired cages placed in both sides of the apparatus contained different stimuli. In the pre-test, two identical nonsocial stimuli (folded white papers) were placed in the wired cages, the locomotion and position preference of the mouse were recorded. In the social preference test, a toy brick and an unfamiliar male conspecific (6 weeks old) were put in the wired cages with the object cage positioned on the preferred side. In the social novelty preference

test, the toy brick was replaced by a novel male mouse, while the other cage contained the familiar mouse. There was a 45-min interval between different test sessions. The time spent in the zone near each cage (head distance less than 5 cm) was considered as interaction time, and the time spent in circular locomotion was excluded from the total time. Mice with circular locomotion longer than half of the test time were excluded. The social preference index was calculated as a ratio of (t_{mouse} - t_{object}) to (t_{mouse} + t_{object}), and novelty preference index was calculated as a ratio of ($t_{stranger}$ - $t_{familiar}$) to ($t_{stranger}$ + $t_{familiar}$).

Social novelty recognition test

Mice showing no obvious aggressive behavior were used in the social novelty recognition test. After 4 hr of social isolation, a male stranger mouse (6-7 weeks old) was introduced into the home cage of the test mouse, with the grid top, food, and water bottle removed, and the mice were allowed free social interaction for 2 min. Then the intruder mouse was taken away immediately. The whole testing procedure was composed of 6 trials with an interval of 10 min. From trial 1 to trial 5, the same intruder (stranger 1) was presented to the test mouse, whereas a novel mouse (stranger 2) from a different cage was introduced in trial 6. Duration of proactive social interaction was manually timed. Social recognition index was calculated as the time difference of proactive social interaction duration in trial 6 and trial 5 (T_6 - T_5). Blind statistical analysis was performed by an experienced experimenter.

In vivo levodopa treatment

Levodopa and benserazide (Sigma) (L/B, 4:1 mass ratio) were thoroughly dissolved in saline just before the tests. Mice received intraperitoneal injections of L/B solution or an equivalent volume of saline. This treatment was carried out one week apart with a 3-day habituation period before the day of test. Half of the animals were initially administered saline in the first week of test and then L/B in the second week, while the remaining half received L/B in the first week and saline in the second week. The drug or vehicle was intraperitoneally injected 10 min before the first behavior test daily. Behavior tests of these animals included open field test, elevated plus maze test, social preference test, and social novelty preference test, as described above. In the social novelty recognition test, each control or *gRNA* mouse (*Dat*^{cre}::*Cas9*^{fl} mice with virus injections) was tested only once, receiving either saline or 20 mg·kg^{-1} L/B. The intervals in social preference/novelty test and the social novelty recognition test were shortened to 20 min and 5 min, respectively, to ensure that all tests were completed within 60 min after the pharmacological treatment.

Fiber photometry of dopamine release

To monitor the real-time dopamine release in NAc core during social interaction, we injected AAV-hSyn-rDA3m into the NAc core (300 nl, coordinates relative to bregma in mm: AP +1.09, ML -1.10 or +1.10, DV -4.60). In *Scn2a* floxed mice, AAV-TH-Cre-EGFP or AAV-TH-EGFP was injected into the VTA along with AAV-hSyn-rDA3m to the NAc core. In *Dat*^{cre}::*Cas9*^{fl} mice, AAV-hSyn-rDA3m was injected to NAc four weeks after the injection of AAV-*gRNA*-EGFP or AAV-*ΔgRNA*-EGFP to the VTA. In WT and *Scn2a*$^{+/-}$ mice, AAV-hSyn-rDA3m was injected to NAc, together with AAV-*ΔgRNA*-EGFP (mixed viruses 9:1) in some mice that allowed EGFP expression serving as a reference fluorescence signal. Fiber optic cannula (Inper; 200 μm in diameter, 0.50 NA) was implanted to the NAc core 200 μm above the injection site. Two anchoring screws were implanted in the skull without damage to the brain. We then secured the cannula and cranial screws with Loctite 4305 UV-curing adhesives and dental cement.

Behavior tests were carried out 2-4 weeks after the AAV-hSyn-rDA3m injection. Before the tests, a mono optic fiber was continuously irradiated with the highest power to minimize the effects of autofluorescence. We then connected the cannula to a multi-channel fiber photometry system (ThinkerTech) through the optic fiber. The dopamine rDA3m sensor was excited by a 580-nm LED light source at 40 Hz (10 ms in pulse duration) with a power of ~50 μW (tested during constant light). After recording in each behavior test, we also obtained the offset of the recording system (F_{offset}) by putting the fiber tip in dark, i.e., the fluorescence intensity value detected by the system with the same parameters used during recording. Fluorescent signals (F and F_0) were obtained by subtracting F_{offset} from the recorded fluorescence intensity in the target brain region. As rDA3m sensor lacks isosbestic point,[43] we simultaneously recorded EGFP fluorescence as a reference to monitor motion artifacts.[85] Due to the low background autofluorescence of long-wavelength channel and the high signal-to-noise ratio of rDA3m sensor, no correction procedure was applied, consistent with other works involving red sensors.[86,87]

We used the CED Micro1401-3 and Spike2 software to trigger the fiber photometry system and a top-view camera and thus synchronize both optic signal acquisition and videotaping animal behaviors. A side-view recording camera was also utilized to aid in behavior judgment. The test mouse was introduced to a transparent acrylic box (35 cm × 35 cm × 35 cm) or underwent similar procedure of the social novelty recognition test mentioned above with the external optic fiber connected. After a 10-min habituation, the recording was started with an initial 3-min collection of baseline signals. A junior male mouse was then put into the box or the cage for free social interaction for another 5 min.

The behaviors of the mice were inspected frame by frame. Social interaction events are defined as direct nose-tip contacts with the head or body trunk of the social target. The beginning of each bout of social interaction is defined as the first frame of direct contacts. Two contacts with interval less than 2 s are considered as one bout of social interaction. Aligning these events with fiber photometry signals allowed the extraction of changes in rDA3m signals (reflecting changes in dopamine levels) before and after each active interaction bout. We employed the adaptive iteratively reweighted penalized least squares to cope with the fluorescent bleaching and thus achieve the baseline correction (MATLAB code from ThinkerTech). The change in dopamine release was calculated as the ratio of (F - F_0) to F_0, i.e., $\Delta F/F_0$, where F_0 is the average fluorescence value 2 s before each bout or during the initial 3 min. Adaptation index

Please cite this article in press as: Li et al., Selective loss of *Scn2a* in ventral tegmental area dopaminergic neurons leads to dopamine system hypofunction and autistic-like behaviors, Neuron (2025), https://doi.org/10.1016/j.neuron.2025.06.003

in Figure 4N was calculated as the $\Delta F/F_0$ difference between the first two active interaction (1^{st} - 2^{nd}). Recognition index of dopamine release was calculated as the $\Delta F/F_0$ difference between trial 6 and trial 5 ($Trial_6$ - $Trial_5$).

In experiments assessing basal dopamine levels, we conducted continuous recordings of dopamine signals 20 min before and after SCH intraperitoneal injection in WT and *Scn2a*$^{+/-}$ mice. Considering the rate of photobleaching stabilized to an approximately linear trend between 15 to 40 min after the onset of recording, a linear fitting approach (applied to the window from 10 to 20 min after drug application) was employed to eliminate the effects of bleaching. The fitting curve was then subtracted from the fluorescence trace to obtain ΔF. F_0 was calculated as the average fluorescence intensity in the window from 10 to 20 min post injection. Basal dopamine levels were quantified by the area under the curve (AUC) of $\Delta F/F_0$ during the 5-min period preceding SCH injection.

In vivo optogenetic stimulation

To assess the impact of L/B on dopamine release in response to optogenetic stimulation of VTA DANs, we activated VTA neurons by blue light and employed fiber photometry to monitor dopamine level in NAc core. Stereotactic injection of viruses was performed in WT or *Scn2a*$^{fl/fl}$ mice at the age of 4 weeks. We bilaterally injected a mixture of AAV-TH-Cre and AAV-DIO-ChR2-EYFP in VTA to allow the expression of ChR2 in *Th*$^{+}$ neurons. The AAV-hSyn-rDA3m was injected into the right NAc core. Two cannulas (Inper; 200 μm, 0.50 NA) were implanted 200 μm above the injection sites of the right hemisphere, respectively. The imaging experiments were carried out 5 weeks after the virus injection. During the experiments, the mouse was securely head-fixed on a floating foam ball with proper airflow to ensure flexible movements.

We utilized a mono optic fiber to connect the NAc-cannula to the fiber photometry system, and another optic fiber to connect the VTA-cannula for light stimulation. For fiber photometry recording, to prevent temporal overlap between interleaved optical stimulation and DA sensor imaging, we chose a lower sampling rate for photometry at 20 Hz. For optogenetic stimulation, we delivered a 470-nm laser beam (ThinkerTech) to VTA DANs with bursts of light pulses (20 Hz, 10 ms each pulse, 2-s burst duration) every 3 min. The first burst stimulation commenced after the mice adapting for 10 min. Intraperitoneal injection of saline or L/B was carried out 1 min after the third burst stimulation. Signals were recorded for a time period of 107 min including 17 min baseline (before treatment) and 90 min post treatment.

We observed two obvious effects of L/B treatment on dopamine signals, one is a long-lasting increase in the baseline dopamine level (up to 60 min), and the other is the enhancement of dopamine release evoked by light stimulation (Figures 6A–6D). The baseline changes of rDA3m were quantified as the AUC of $\Delta F/F_0$, with the evoked signals and the bleaching trend removed. Specifically, we removed the light-evoked signals by deleting data points from 5 s before to 30 s after the stimulation. For fluorescence bleaching effects of rDA3m signals, we fitted the signals before injection and 90 min after injection with a double exponential decay function to obtain the decay curve. Then the fitting curve was subtracted from the whole trace of rDA3m signals. The resulting signals were then converted to $\Delta F/F_0$ to calculate the AUC, where F_0 was the average fluorescence intensity before injection. Similar analysis was used to quantify the effects of SCH treatment on rDA3m sensors (Figures S11K and S11L). For the light-evoked dopamine release, $\Delta F/F_0$ after the start of the light stimulation (a period of 30 s) was calculated, where F_0 is the average intensity within the period of 5 s before the stimulation. For group data, the evoked rDA3m signals were normalized to the signals before saline or L/B treatment for each recording.

QUANTIFICATION AND STATISTICAL ANALYSIS

We analyzed the data using MATLAB (R2017b and R2022a, MathWorks), Spike2 software (CED), and GraphPad (Prism 9 and 10). The amount of data required for individual experiments was not calculated before the test. All experiments were performed blindly to the groups except slice recording in mPFC and recordings from isolated blebs in NAc. All data were analyzed in a blinded manner. All measurements were taken from distinct samples unless otherwise stated. We used Shapiro-Wilk test to check the normality of the samples. We performed two-tailed unpaired t test for independent samples with normal distribution, and Mann-Whitney U test for samples with non-normal distribution. One-way ANOVA was applied when there was one independent variable with more than two categories. When there were two independent variables, two-way ANOVA was used. To determine statistical significance in comparisons, we set the alpha value at 0.05. *$p < 0.05$, **$p < 0.01$, ***$p < 0.001$. The experimental data in the text and figures were described as mean ± s.e.m.